CENTRO INTERNACIONAL DE ESTUDOS
DE DOUTORAMENTO E AVANZADOS
DA USC (CIEDUS)

TESIS DE DOCTORADO

# LAGRANGIAN AND INERTIAL TRANSPORT IN ATMOSPHERIC AND CHAOTIC FLOWS

Angel Daniel Garaboa Paz

**ESCUELA DE DOCTORADO INTERNACIONAL**

**PROGRAMA DE DOCTORADO EN Ciencias Marinas, Tecnología y Gestión**

SANTIAGO DE COMPOSTELA

AÑO 2018

USC
UNIVERSIDADE
DE SANTIAGO
DE COMPOSTELA

# DECLARACIÓN DEL AUTOR DE LA TESIS

**Lagrangian and inertial transport in atmospheric and chaotic flows**

D./Dña. Ángel Daniel Garaboa Paz

*Presento mi tesis, siguiendo el procedimiento adecuado al Reglamento, y declaro que:*

1) *La tesis abarca los resultados de la elaboración de mi trabajo.*
2) *En su caso, en la tesis se hace referencia a las colaboraciones que tuvo este trabajo.*
3) *La tesis es la versión definitiva presentada para su defensa y coincide con la versión enviada en formato electrónico.*
4) *Confirmo que la tesis no incurre en ningún tipo de plagio de otros autores ni de trabajos presentados por mí para la obtención de otros títulos.*

*En Santiago, de de 2018*

Fdo. Angel Daniel Garaboa Paz

USC
UNIVERSIDADE
DE SANTIAGO
DE COMPOSTELA

# AUTORIZACIÓN DEL DIRECTOR / TUTOR DE LA TESIS

**Lagrangian and inertial transport in atmospheric and chaotic flows**

D. Vicente Perez Muñuzuri
D. Florian Huhn

INFORMAN:

*Que la presente tesis, corresponde con el trabajo realizado por D/Dña.* ***Ángel Daniel Garaboa Paz****, bajo mi dirección, y autorizo su presentación, considerando que reúne los requisitos exigidos en el Reglamento de Estudios de Doctorado de la USC, y que como director de ésta no incurre en las causas de abstención establecidas en Ley 40/2015.*

*En Santiago, a de de 2018*

Fdo. Vicente Perez Muñuzuri

Fdo. Florian Huhn

USC
UNIVERSIDADE
DE SANTIAGO
DE COMPOSTELA

*Caminante, son tus huellas*
*el camino, y nada más;*
*caminante, no hay camino,*
*se hace camino al andar.*
*Al andar se hace camino,*
*y al volver la vista atrás*
*se ve la senda que nunca*
*se ha de volver a pisar.*
*Caminante, no hay camino,*
*sino estelas en la mar.*

*Antonio Machado*

USC
UNIVERSIDADE
DE SANTIAGO
DE COMPOSTELA

# Contents

# Acknowledgments

Sin lugar a dudas, la tesis es una de las etapas más duras a la que toda persona que quiere hacerse un hueco en el mundo de la ciencia tiene que enfrentarse. En el libro de Steven Strogatz: ”Nonlinear dynamics and Chaos”, los problemas más complejos están en un lugar especial separados del resto. Creo que la tesis doctoral encajaría perfectamente en este lugar. Sin embargo, a diferencia de los otros problemas, a este sí que le encontré solución y fue tan sencillo como rodearme de los mejores, por lo que sólo me queda agradeceros a todos vuestro apoyo en esta aventura.

En primer lugar, dar las gracias a mi director de tesis, Prof. Vicente Perez Muñuzuri, por darme la oportunidad de iniciarme en el mundo de la investigación, por todo lo aprendido de él dentro y fuera del mundo científico y por su consejo y comprensión durante estos años. A mi codirector, el Dr. Florian Huhn, por ser mi mejor consejero personal y apoyarme durante mi estancia en Göttingen. Al Prof. Gonzalo Míguez Macho, por su ayuda desde que llegué al GFNL y por su tranquilidad cuando más la necesitaba. Gracias a los Profs. Alberto Pérez Muñuzuri y Nieves Álvarez.

I want to thank Drs. Andreas Schröder and Daniel Schanz from the German Aerospace Center (DLR), and also to Dr. John Lawson, and the technical staff from the Max Planck Institute for Dynamics and Self Organization (MPIDS), for their guidance during my research stay in Göttingen. I thank Profs. Cristobal Lopez, Emilio Hernández and Dr. Joao Bettencourt, from the Instituto de Física Interdisciplinar y Sistemas Complejos (IFISC) for their support during my research stay in Mallorca. I thank to the Spanish Ministery of Education and Science and the European Commission for they financed this research.

Dar infinitas gracias mis compañeros de laboratorio, que hacen que este trabajo sea mucho más agradecido todos los días y con los que compartí fútbol, vicios, churrascos, fiestas, cafés, charlas y congresos. A Charlie-Python, el núcleo del GFNL, por su templanza y su buen carácter, sigue conservando el título a la persona más buena del mundo. Al Dr. Eiras 24/7, nuestro alférez, por ser un hombre de acción, que empezó esta aventura conmigo y por todas las risas que dio. A Mikel, la organización y el pragmatismo, el mejor trabajador que tiene y tendrá el GFNL durante muchos años y a Damián, nuestro mejor centro meteorológico, ejemplo de pasión por la investigación. Gracias a Sabela, Darío, Breogán, Irma, Alberto, David, Sara, Ana y Marianmo, y a nuestros otros doctores, Alberto, Swen, Jacobo, Alexandre, con los que compartí mis inicios y, aunque no estén aquí, siguen siendo miembros del GFNL.

Gracias a todos mis amigos, por ser la mejor distracción cuando la presión más apretaba: Manolo, Javieres, Pepe, David, José, y aquellos que me acompañaron desde la carrera: Diego, Díaz, Pablo, Sergio y Aaron. Gracias a José Vidal, por hacerme ver más allá del trabajo.

Gracias de todo corazón a Andrea, mi mejor compañera de viaje, por ser mi empuje diario sin dejar que me dispersara y ayudar a centrarme; gran parte de esta tesis se la debo a ella. Gracias a mi familia; a mis hermanos, Dora, Ramiro y Carlos, a mis sobrinas, Lucia y Alba,

a mi padre y, muy especialmente, a mi madre, por ser motivación e inspiración para seguir adelante; sin ellos nunca habría llegado aquí.

# Summary

This thesis presents a compendium of publications related to transport studies analyzed from the perspective of dynamical systems. The goal is to address the role that particle properties and the flow have on the organization of trajectories and hence the transport.

To observe how transport is structured, we focus on the most widely used method: the Finite Time Lyapunov Exponents. These exponents measure the separation rate of the particles starting from nearby initial positions, estimating the hyperbolicity of the trajectories. This method allows us to make a first approach to the problem, obtaining the borders or frontiers between regions with different dynamics given a simplified vision of transport. The transport structures related with this method, are called Lagrangian Coherent Structures.

In the first study, the Lagrangian transport in the troposphere was analyzed. The atmospheric flow is characterized by being turbulent in a continuum of spatiotemporal scales. Within these scales, it was observed that there are structures such as the Atmospheric Rivers that maintain a spatial and temporal coherence of the order of days acting as organizers of water vapor transport and therefore dominating the dynamics of the region at the moment they occur. At the same time, the persistence and repetition of these structures, together with all the other tropospheric structures, introduce mixing into the atmosphere. Those areas in middle latitudes where these structures develop have higher mixing variability. This is mainly due to seasonal changes. However, those regions with less variability, such as the equatorial zones, the mixing and its variability on day scales, are mainly associated with inter-annual variability events such as El Niño or La Niña or the Intertropical Convergence Zone (ITCZ). In addition, the mixing information of the air masses from a climatic point of view, was used as a predictor of rainfall for the Iberian region. The Atlantic margin is characterized by an intense activity of Atmospheric Rivers, being one of the main causes of precipitation. However, the problem of determining the activity of rainfall months in advance is complex, for this reason the use of new variables as potential predictors is required. It has been obtained that the mixing, in the Atlantic region, is related to the precipitation on the Iberian Peninsula.

Addressing on the second study, we focus on the influence of forces on the particles motion so the resolution of motion equation is required to obtain the trajectories they describe. The particles are modeled as small spheres with mass, but the fact that their movement is decoupled from the flow makes their trajectories depend initially on other properties such as the initial velocity. It was observed that this dependence, for certain flows, is even higher than small perturbations in its position, mainly in those regions where there is a high spatial variability of the fluid such as regions with shear. The same happens for bubbles where flotation effects appear. They are very sensitive to the inertial effects and especially to the disturbances of the radius as well as the effects of merging with other bubbles, being especially relevant in the initial instants of the movement. In addition, it has been observed that particles properties and their collective motion play a key role in the synchronization of finite-size chemical oscillators.

To experimentally support some of the aforementioned behaviors, experimental data are needed to measure the trajectories of the particles. Particle Tracking Velocimetry (PTV) methods, track the trajectories of individual particles in three-dimensional space. In the last part of this thesis, we present an experimental setup and some preliminary results of trajectories of the particles mentioned above in a high turbulent flow.

# Resumen

Esta tesis presenta un compendio de publicaciones relacionadas con distintos problemas del transporte analizados desde la perspectiva de los sistemas dinámicos. El objetivo es estudiar la influencia que las propiedades de las partículas y el flujo tienen en la organización de las trayectorias y, por lo tanto, en el transporte.

Para ver cómo se estructura el transporte, nos centramos en el método más extendido: los exponentes de Lyapunov de tiempo finito (FTLEs, por sus siglas en inglés). Estos exponentes miden la velocidad de separación de las partículas que parten de posiciones inicialmente cercanas, siendo un estimador de la hiperbolicidad de las trayectorias. Este método nos permite hacer una primera exploración del problema, identificando los contornos o fronteras entre regiones con una dinámica diferente, proporcionando una visión simplificada del transporte. Las estructuras del transporte obtenidas con este método se conocen como estructuras lagrangianas coherentes (LCSs, por sus siglas en inglés).

En el primer estudio se analizó el transporte lagrangiano en la troposfera terrestre. El flujo atmosférico se caracteriza por ser turbulento con un continuo de escalas espacio-temporales. Dentro de estas escalas, se observó que hay estructuras, como los ríos atmosféricos, que mantienen una coherencia espacial y temporal del orden de días, actuando como organizadores del transporte del vapor de agua y, por lo tanto, dominando la dinámica de la región mientras ocurren. A su vez, la persistencia y la repetición de estas estructuras, junto con todas las otras estructuras troposféricas, introducen mezcla en la atmósfera. En aquellas áreas en las latitudes medias, donde estas estructuras se desarrollan, hay una mayor variabilidad de mezcla debido, principalmente, a los cambios estacionales. Sin embargo, en aquellas regiones con menor variabilidad, como en las zonas ecuatoriales, la mezcla y su variabilidad en la escala de días viene principalmente asociado a eventos de variabilidad interanual como El Niño, La Niña o la Zona de Convergencia Intertropical (ZCIT). Adicionalmente, la información de la mezcla de las masas de aire desde un punto de visa climático se utilizó como predictor para las precipitaciones sobre la región Ibérica. El margen Atlántico está caracterizado por tener una actividad intensa de Ríos Atmosfericos, siendo una de las principales fuentes de precipitación. Sin embargo, el problema de determinar la actividad de las precipitaciones con meses de antelación es complejo; por este motivo, se requiere el uso de nuevas variables como potenciales predictores. Se ha observado que la mezcla en la región Atlántica guarda relación con la precipitación sobre la Peninsula Ibérica.

En el segundo estudio nos centramos en la influencia que ejercen distintas fuerzas en la dinámica de las partículas; por lo tanto, se requiere la resolución de la ecuación del movimiento para obtener su trayectoria. En una primera aproximación, las partículas se consideran como pequeñas esferas con masa, pero el hecho de que su movimiento esté desacoplado del flujo hace que sus trayectorias dependan inicialmente de otras propiedades, como la velocidad inicial. Incluso, en determinados flujos, esta dependencia es mayor que pequeñas perturbaciones en

su posición, observándose principalmente en flujos con una gran variabilidad espacial, como en zonas con cizalladura. Lo mismo se observó con burbujas, en las cuales existen efectos de flotación, que hacen que las burbujas sean muy sensibles a las variaciones en el radio, así como a los efectos de unión con otras burbujas, siendo especialmente relevantes en los instantes iniciales del movimiento. Además, se ha observado que las propiedades de las partículas y su distribución juegan un papel clave en la sincronización de osciladores químicos.

Para observar experimentalmente algunos de los comportamientos anteriormente mencionados, se necesitan datos experimentales de las trayectorias reales de las partículas. Los métodos de Particle Tracking Velocimetry (PTV), permiten obtener trayectorias individuales de las particulas en un espacio tridimensional. En la última parte de esta tesis, presentamos el montaje experimental y unos resultados preeliminares de trayectorias de partículas, como las mencionadas anteriormente en un flujo altamente turbulento.

# Chapter 1

# Introduction

## 1.1 Motivation

Transport in physics is movement through a medium. It is ubiquitous in the natural world which surround us and spans a spectrum of spatio-temporal scales, stretching from the milk inside a cup of coffee to water droplets, to bubbles or clouds in the air (Fig.(1.1)) or the smoke from a cigarette, or the debris and foam over the sea surface, these, just a few examples.

Nowadays, the increase in technical capacities has enabled tremendous computational and empirical capabilities, allow in to observe and understand transport processes in the same way that we can observe day to day ones with the naked eye. On geophysical scales, thanks to satellite imaging, we can observe the movement of the atmosphere and hence the motion of large air masses; the wind, transporting water vapor (Fig.(1.1)b), dust, pollution or temperature, or the movement of global water masses; the ocean currents transporting plankton, salt and temperature. At much smaller scales we can observe the motion of blood inside our vessels, transporting nutrients or also the motion of microparticles inside high turbulents flows. All these transport processes condition our environment and our daily-life.

In the last few years, many catastrophic events related to transport have grabbed the attention of the media. In March 2011, in Japan, due to at the Great Tohoku earthquake and the resultant tsunami Cs-137 radionucleids were released into the sea, exposing marine ecosystems to radioactive materials. Computer simulations and ocean drifters have measured the impact of the large scale ocean currents on the radionucleids, showing they are spread over the whole Pacific Ocean with very high concentrations at the source point, the Fukushima nuclear plant [1, 2, 3]. The waters surrounding the Fukushima nuclear plant are closed, and fishing or any other kind of marine activity is not allowed.

Also, on March 7 2014, the flight MH370 from Malaysia Airlines accident, which provoked an intensive search to find the wreckage of the plane in the Ocean, without success in the following days [4]. The search was particularly hard due to the unknown location of the crash landing, the heterogeneity of the pieces found, transport by ocean currents and the sinking of the wreckage, all these increased its difficulty [5]. Only 17 months later it was possible to find small parts of the plane in Madagascar and Mozambique, thousands of kilometers away from the estimated crash site.

This example shows the well known chaotic behavior of turbulent flows introduced by Lorenz (1963) [6]; despite the well located origin of source material source, the advection by ocean currents and the presence of different forces cause small disturbances in initial

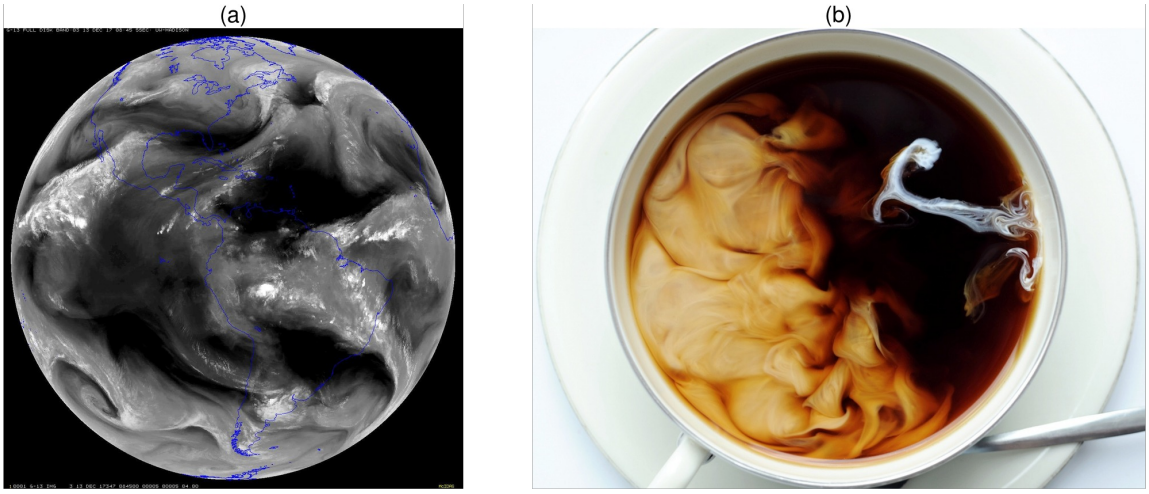


Figure 1.1: (a) Global pattern of water vapor obtained from Satellite Himawari-8 (Japan Meteorological Agency). (b) Mixing pattern process of milk and coffee in a cup.

conditions to lead to very different destinations, making understanding the transport topology exponentially harder.

In the case of radionucleids, the concentration is many orders of magnitude smaller than the surrounding water volume, so the physical properties such as size and density are irrelevant in terms of transport. Its transport will be completely determined by the surrounding amount of water mass and the oceanic currents behaving like a tracer of motion of fluid. Thus, the transport of the radionucleids and water masses are totally coupled. For the plane case, the size and the density of the material are many orders of magnitude higher than the surrounding water molecules, so its motion cannot be approximated in the same way. Gravity, buoyancy and drag effects among others, completely change its trajectory with respect to the surrounding water masses. In this case, the transport of the wreckage and the water masses are uncoupled.

Despite being different events, they share a common frame: there is a free substance or a material in a given flow and to know which is its final destiny is a key problem to address, to prevent catastrophic consequences or at least try to be ahead of them [7]. The challenges are the number of degrees of freedom, non-linearity and chaotic behavior due to the sensitiveness to initial conditions. Thus, simulating all possible scenarios for a given event to obtain useful results turns into a overwhelming task. The simplification of transport understanding, extracting the key information and obtaining the template that organizes the motion is the concern of dynamic system theory. It focuses on the analysis of trajectories and the evolution rather than understanding the fluid dynamics from a physical point of view. The main goal is to locate or segregate these groups of trajectories according to their particular dynamics and hence allow the understanding of a destination for the substance or material transported.

In this thesis, we will mainly focus on Lagrangian based measures which explicitly track motion, in order to define those templates organizing transport that remain relevant in space and time. These are coordinate-frame invariant, and perhaps most importantly convey information regarding fundamental mechanisms of transport.

## 1.2 Transport processes: Advection and diffusion

In nature, like the examples cited in Sec. (1.1), the transport of a scalar property $C(\mathbf{r},t)$ at a given position $\mathbf{r}$ and at a given time $t$, from one location to another is mostly driven by the combination of two physical processes: *diffusion* and/or *advection*.

**Diffusion** is an irreversible process due to the molecular random walk motion and it has its origin in the gradient concentration. As a consequence of this gradient, there is a net flux of mass transfer from the region with higher concentration to the lower one. Molecular collective motion is modeled as a continuum quantity, $C(\mathbf{r},t)$, expressed by Fick's first law,

$$J(\mathbf{r},t) = -D_m \cdot \nabla C(\mathbf{r},t), \tag{1.1}$$

where $J(\mathbf{r},t)$ is the diffusive flux and $D_m$ is the diffusion coefficient which measure the rate of the diffusion process and depend on the medium properties. From the mass continuity equation,

$$\frac{\partial C(\mathbf{r},t)}{\partial t} + \nabla J(\mathbf{r},t) = 0 \tag{1.2}$$

and Eq. (1.1), we can derive Fick's second law,

$$\frac{\partial C(\mathbf{r},t)}{\partial t} = D_m \nabla^2 C(\mathbf{r},t). \tag{1.3}$$

**Advection** is the physical process that governs variations $C(\mathbf{r},t)$ by the effect of the bulk motion of fluid. In Cartesian coordinates this process is described by,

$$\frac{\partial C(\mathbf{r},t)}{\partial t} + \mathbf{v}(\mathbf{r},t) \cdot \nabla C(\mathbf{r},t) = 0 \tag{1.4}$$

where $\mathbf{v}$ is the flow velocity field. Both processes can be combined,

$$\frac{\partial C(\mathbf{r},t)}{\partial t} = D_m \nabla^2 C(\mathbf{r},t) + \mathbf{v}(\mathbf{r},t) \cdot \nabla C(\mathbf{r},t). \tag{1.5}$$

## 1.3 Lagrangian and Eulerian frames

In the previous section, the variation on a scalar quantity $C(\mathbf{r},t)$ is described in terms of a function in time and space. The variation of this scalar quantity can be expressed by two different frames or points of view. The Eulerian and the Lagrangian frames.

Using real word examples, the Eulerian frame description is the equivalent of having a net of fixed buoys on the sea surface with a sensor measuring a property $C$ at a given position $\mathbf{r}$ and at a given time $t$, described by a function $C(\mathbf{r},t)$. This field description gives instantaneously the rate of change, such as the variation of the velocity field $\mathbf{v}(\mathbf{r},t)$.

The other intuitive option is the Lagrangian frame. Following the previous example, the buoys can be released and permitted to be carried by the flow, tracking them as single particles and measuring the quantity $C(\mathbf{r},t)$ along the trajectory described by $\mathbf{r} = \mathbf{r}(t)$. This point of view is the Lagrangian one, so each initially tagged buoy is a representation of an initial fluid parcel, and $\dot{\mathbf{r}}$ is the velocity at each point along a trajectory of the corresponding fluid element,

$$\dot{\mathbf{r}} = \frac{\partial \mathbf{r}}{\partial t} = \mathbf{v}(\mathbf{r},t). \tag{1.6}$$

The goal of the Lagrangian analysis is to understand the motion and evolution of objects, matter, or properties that are carried along by the flow and any property derived from the integrated fluid motion, as opposed to an instantaneous Eulerian snapshot, where the conclusions are taken from instantaneous information causing a misleading perception of the integrated motion over time.

The material derivative $DC(\mathbf{r},t)/DT$ is the rate of change of a scalar property or function $C(\mathbf{r},t)$ following a tagged fluid motion as it moves throughout the flow field,

$$\frac{DC(\mathbf{r},t)}{Dt} = \underbrace{\frac{\partial C(\mathbf{r},t)}{\partial t}}_{\text{Local rate of change}} + \underbrace{\mathbf{v}(\mathbf{r},t)\cdot\nabla C(\mathbf{r},t)}_{\text{Advective change}}. \tag{1.7}$$

If the scalar field is materially conserved (there is no source or sinks for $C$) then its material derivative must vanish, and $C$ must satisfy the scalar advection equation (1.4) along the trajectory described by the tagged element,

$$\frac{DC(\mathbf{r},t)}{Dt} = 0. \tag{1.8}$$

Equation (1.8) expresses the principle that the motion and evolution of a materially conserved property are completely determined by the fluid trajectories. However, in any real fluid, it is not exact, since molecular or turbulent diffusion will also influence property distributions.

Also, the connection between a Lagrangian tracer and the scalar field occurs when a particle just follows the fluid particle elements due to the action of fluid bulk motion. However, in real life and regarding to the buoy problem, this is not the case (see above).

The focus of the present text is purely on the advection and inertial motion, and diffusive effects are therefore neglected.

## 1.4 Transport scales

The spatio-temporal scales define the physical dimension of a magnitude in space and time of an object or a process. To estimate them allows us to make simplifications and also to determine the role of any main key process.

Considering the characteristic scales involved in diffusion and advection processes: $U, C, L$ and $D_m$, which are respectively, the characteristic velocity, concentration, length, and diffusion velocity, we perform a dimensional analysis of Eq. (1.4),

$$\mathbf{v}(\mathbf{r},t)\cdot\nabla C(\mathbf{r},t) \approx U\frac{C}{L} \quad , \quad D_m\nabla^2 C(\mathbf{r},t) \approx D_m\frac{C}{L^2} \tag{1.9}$$

and comparing both processes, the ratio of their scales is,

$$\frac{advection}{diffussion} = \frac{UC/L}{D_m C/L^2} = \frac{UL}{D_m} = Pe. \tag{1.10}$$

This ratio is the Peclet number and it relates the diffusion speed with the advection velocity. For transport processes with $Pe \gg 1$, the advection is the main transport mechanism and the diffusion can be neglected. When $U$ and $L$ increase, the Reynolds number $Re = UL/\nu$ also increases. There is an energy cascade from higher spatio-temporal scales $L$, (injection scales) to the smaller ones (Kolmogorov scales, $\eta$), creating flow structures and increasing the flow variability. In fluid regimes with a high Peclet number, these flow structures dominate the large scale advection over diffusion.

This work is mainly concerned with fluid flows with the characteristic scales range between liquids and gases with a $D_m \in [10^{-5}, 10^{-1}]\,\mathrm{cm}^2/\mathrm{s}$) respectively; a characteristic range speed $U \in [0.1, 7.8]\,\mathrm{m}^2/\mathrm{s}$, and characteristic length $L \in [10^{-6}, 10^{6}]\,\mathrm{m}$. Thus, we are on a regime $Pe \gg 1$ so diffusive effects can be neglected.

When we move from a Lagrangian tracer, to a real particle the presence of inertial effects compete with the bulk motion of water masses due to advection. The particle also has an inner characteristic time, $\tau_p$, the relaxation time. It is defined as the time required by the particle to respond to changes in the flow field. This, together with $U/L = T$, the characteristic time flow scale, defines another dimensionless number. The Stokes number,

$$St = \frac{\tau_p U}{L} = \frac{\tau_p}{T}. \tag{1.11}$$

This measures the degree of coupling between the particle and the fluid. If the Stokes number is small, $St \ll 1$, the particle motion is tightly coupled to the fluid motion and hence the particles will behave as Lagrangian particle. Such particles are typically being used for quantitative flow measurements. If $St \gg 1$, the particle is not so influenced by the flow and its response time is longer than the characteristic time of the flow so its motion is dominated by its inertia.

The problems looked at in this work will span a range of $St$ regimes, considering transport processes due to inertial and Lagrangian motion.

## 1.5 Dynamical system approach to transport problems

The dynamical systems theory with lead with systems that evolve in time. This perspective considers any particle as a vector $\mathbf{r} = (x_1, ..., x_n)$ describing a *state* with a number of $d$ independent variables under the action of a dynamical system $\mathbf{f}(\mathbf{r}) = (f_1(\mathbf{r}), ..., f_n(\mathbf{r}))$ being the source of change on $\mathbf{r}$ [8]. The evolution of the state is described by a set of nonlinear ordinary differential equations (hereafter, ODEs),

$$\frac{d\mathbf{r}}{dt} \;=\; \dot{\mathbf{r}} \;=\; \mathbf{f}(\mathbf{r}). \tag{1.12}$$

In terms of transport the state $\mathbf{r}$ describes, the particle position and/or velocity at a given time instant and $\mathbf{f}$ is a source of change in the state; the flow action $\mathbf{v}(\mathbf{r})$ and/or any forces applied to the particle.

To find a solution for Eq. (1.12) starting from an arbitrary initial condition $\mathbf{r}(t_0) = \mathbf{r}_0$, we set an imaginary particle and watch its evolution. As time goes on, the particle evolves and the sequence of states based at $\mathbf{r}_0$ represents the particle trajectory. With the initial time $t_0$ and a final time $t$, we can define the *flow map* $\phi_{t_0}^{t}$ as the map function which takes the particle $\mathbf{r}_0$ and evolves it to $\mathbf{r}$ according to Eq. (1.12),

$$\begin{aligned} \phi_{t_0}^{t} \quad &: \quad \mathbb{R}^n \longrightarrow \mathbb{R}^n \\ \mathbf{r}_0 &\longmapsto \mathbf{r}. \end{aligned} \tag{1.13}$$

The analysis of the trajectories concerning their destinations, their organization depending on initial conditions and the phase map, belongs to dynamical systems theory. The information should be summarized to reveal those features which help us to understand how the motion is organized, or in other words, the template that organized the trajectories. In terms of dynamical systems, the picture that summarizes qualitatively different trajectories of the system, is called a *phase portrait*.

The *fixed points* are those points, $\mathbf{r}^*$ where the system solution will be the trivial solution, $\mathbf{f}(\mathbf{r}^*) = 0$, which means in terms of transport that, there is no motion, and the state remains invariant. The fixed points are very important for steady incompressible fluid flows (the stagnation points) due to the fact that they define the so-called invariant manifolds. These are separatrices, segregating those regions with similar dynamics and providing the structures which organize the trajectories. A more formal definition of these points and their associated manifolds will be given in the next chapter.

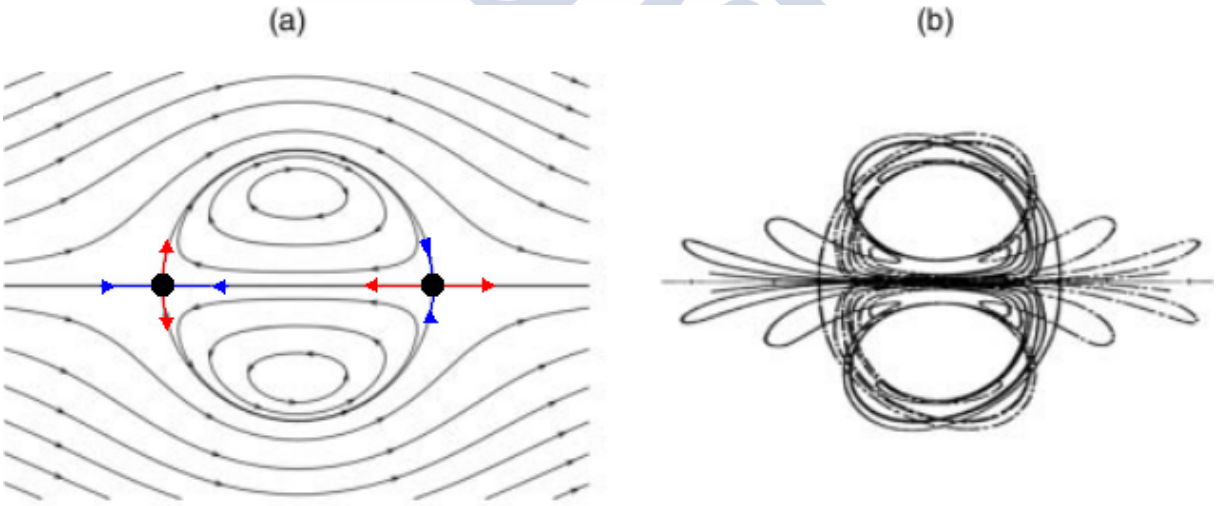


Figure 1.2: (a) Streamlines for a steady vortex dipole. Two hyperbolic saddle-type stagnation points (black dots) with their associated stable (blue) and unstable manifolds (red). The heteroclinic connections behave as separatrices partitioning the flow into regions of distinct dynamics. (b) Heteroclinic tangle formed by transverse intersection of stable and unstable manifolds when a periodic perturbation is applied to the steady vortex dipole. Figure modified from [9, 10]

In practical applications, most real problems are time-dependent and/or three-dimensional and the flows are not integrable. This introduces additional handicaps, making it exponentially more difficult, just for the two-dimensional unsteady (time-dependent) system. In Fig. (1.2), we show how a simple periodic perturbation applied to the fixed points turns the associated invariant manifolds from heteroclinic connection to complex heteroclinic tangles, where the invariants intersect, being the hallmark of chaos [9].

The equivalent of these invariant manifolds for time dependent systems have fallen under the broader category of Lagrangian Coherent Structures (LCS), a terminology adopted from Haller and Yuan [11]. The definitions and relevancy of these invariants are not obvious, and research in this area continues to advance, improving the description, and categorization, while maintaining a practical methodology for revealing "effective " stable and unstable manifolds [9].

In the following subsection, we will describe the transport problems we have examined in this thesis using the approach presented above.

### 1.5.1 Advective Transport in the atmosphere

The atmosphere is a semi-transparent gas of variable composition interacting with the Earth surface under the influence of gravity, rotation and heat from solar radiation. The temperature gradient activates the fluid motion and an energy cascade from thousands of kilometers to less than millimeters, creates flow structures, spanning a spectrum of unsteadiness, leading to different atmospheric phenomena around the globe like the jet stream, storms, hurricanes, monsoons, trade winds... Being the engine of global atmosphere circulation which shapes the global wind patterns (Fig.(1.3)(a)) and responsible for tropospheric mixing. The transport by the fluid advection, between persistent organized structures, is often the primary process shaping tracer patterns and turbulent diffusion, as well as sinks and sources of the tracer which are secondary.

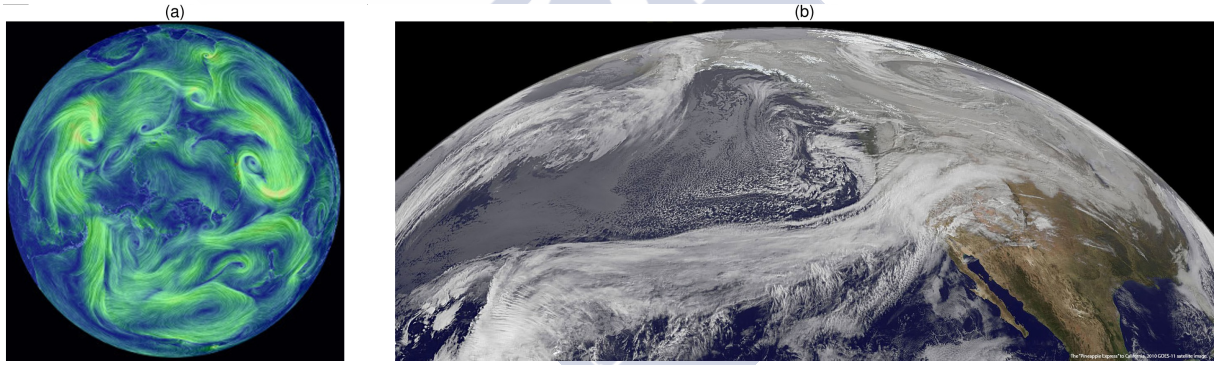


Figure 1.3: (a) Global wind streamlines colored in green for a fixed time in the wind flow field (Cameron Beccario, earthschool.net). (b) Satellite image of Atmospheric River event (National Oceanic and Atmospheric Administration,(NOAA))

The computation of invariant manifolds for the estimation of mixing has previously been used by [12, 13, 14] for the detection of coherent structures in different models of atmospheric flows, such as a zonal stratospheric jets [15], a jet-stream [16], a hurricane [17], transient baroclinic eddies [14] and the polar vortex [18]. More recent studies have used this approach to study atmospheric mixing [15], the polar vortices [19, 20] and also the transport related with hurricanes/cyclones [21, 22, 23, 24] and ocean and atmospheric [25] contaminants.

The persistence and repetitiveness of well defined and isolated flow structures make them suitable for statistical analysis in order to answer the following questions. What is the average activity of the folding and stretching air parcels in a climate period? How does the deformation of the air parcels increase over a climate period? Is the mixing modified due to the seasonal cycle? What is the role that the invariant manifolds play in atmosphere mixing? A case study is

useless, so the use of statistics over several events is required to move from a Lagrangian case study to a statistical Lagrangian approach in the same way that statistical analysis of Eulerian weather variables provide information about climate.

Here, we focus on the motion of air masses in the troposphere, more specifically on the mesoscale. We will pay attention to a particular jet flow structure: Atmospheric Rivers (Fig.(1.3)(b)). These meteorological phenomena are defined as elongated regions of Integrated Water Vapor column (IWV) over 2 cm and winds stronger than 12 m/s, that transport moisture in the lower troposphere close to the 850 hPa level [26, 27, 28]. They have a jet shape propagating from lower to medium latitudes carrying high amounts of water vapor and latent heat, being a key mechanism to redistribute the heat around the globe. More than 90% of poleward water vapor is transported by these elongated structures (longer than 2000 km and narrower than 1000 km), mostly within the Warm Conveyor Belt (WCB) ahead of cold fronts and within the Low Level Jet (LLJ) of extratropical cyclones, these being commonly associated with the polar front [29, 26]. The connection between extreme precipitation and flood events has been shown over the Western Coast [28] of the US and over Europe [30].

### 1.5.2 Inertial particles

In the previous section, to study transport in the atmosphere, we focus on the analysis of fluid particles themselves as ideal tracers in the flow. However, when a finite size particle such as examples shown in Fig. (1.4) moves in a medium, the flow is one of the sources of motion among other forces due to finite size effects such as density, size, etc. Requiring the solution of the motion equation for each individual particle. The inertial particle motion is a dynamical system with dissipative and/or dumping effects and therefore it is not conservative, so there is not preservation of phase space volumes, allowing its contraction and/or expansion. This leads to preferential concentration, clustering and separation of particles which have important implications in natural phenomena.

During the last years, the dynamics of inertial particles have been studied in many research fields such as; sedimentation processes [31], turbulent flows [32], rain generation [33, 34], composite materials [35], volcanic ash transport [36], pollutants and pathogenic spores in the atmosphere [37, 38] and the formation of planetesimals in the early Solar system [39]. Also, other processes, dust transportation from soil erosion, combustion and the mixing of sprays.

### 1.5.3 Lagrangian Particle Tracking

For previous problems, we have considered the solutions of Eq. (1.12) to obtain the particle trajectories. Besides this, trajectories can be obtained experimentally through flow visualization techniques and velocimetry methods. This approach, independent of velocity field information, is possible and indeed desirable since it avoids introduction modeling and computational errors. Techniques like Lagrangian Particle Tracking (LPT) also known as Particle Tracking Velocimetry (PTV) allow us to reconstruct the real particle trajectories through a sequence of pictures (Fig.(1.5)(b)), in the same way that the sequences of states of $\mathbf{r}(t)$ give the solution of Eq. (1.12). This experimental procedure shown in Fig.(1.5)(a), consists of tracking individual free particles in a fluid flow. In order to trace the water fluid motion as an ideal Lagrangian tracer, the particles should have a low Stokes number, $St \ll 1$ to avoid inertial effects. With an illumination source applied to the particles, a sequence of pictures is obtained from a

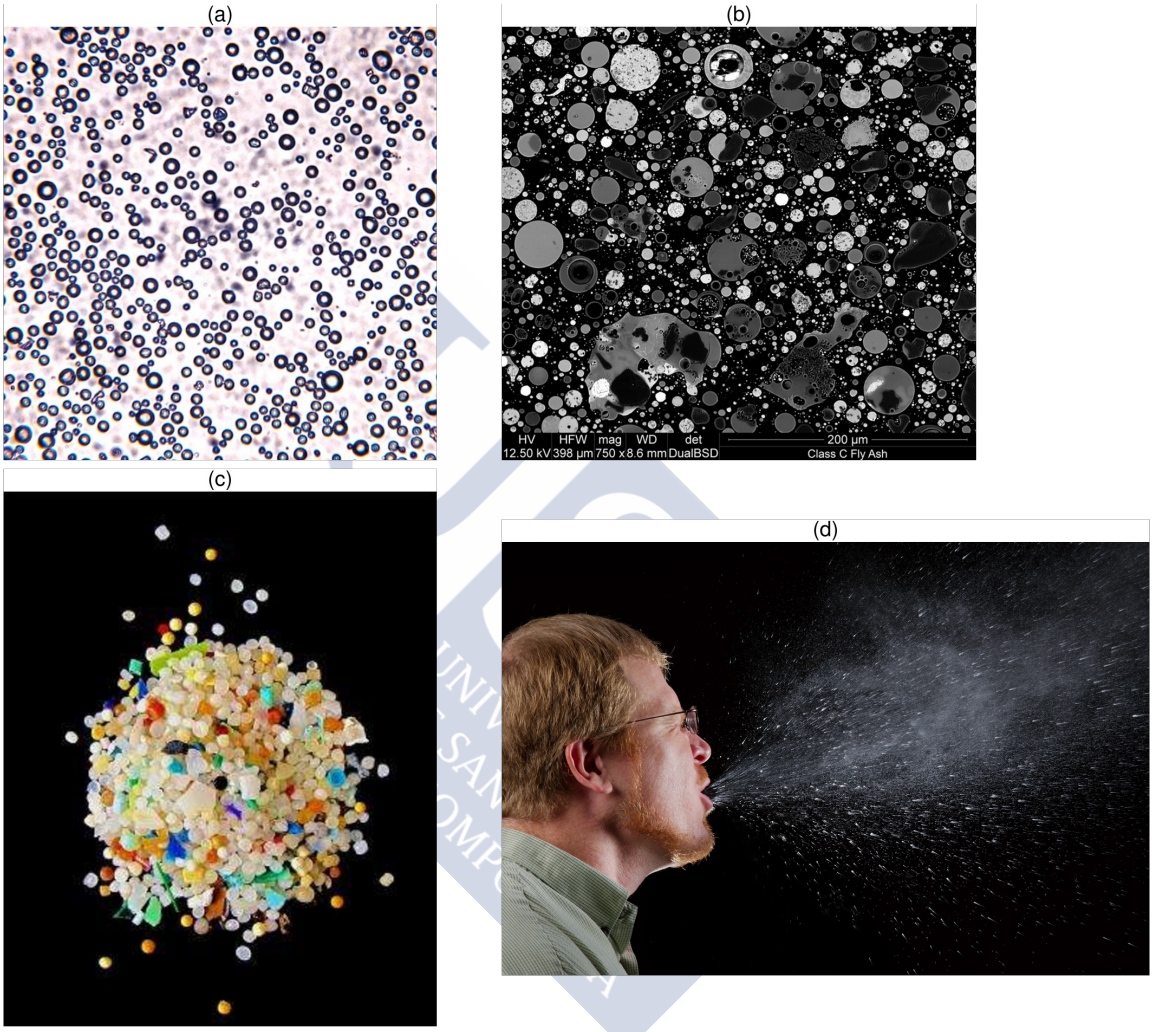


Figure 1.4: (a) Microbubbles under an optical microscope. Medical grade albumin encapsulated gas micro-spheres are imaged with a 20X microscope. Reproduced from [40]. (b) Scanning electron microscopy (SEM) of coal fly ash FA2. Reproduced from [41]. (c) Microscopic fragments of plastic: microplastics. They are pieces of plastic less than 5 mm in diameter and are a global marine pollutant. Reproduced from [42] (d) Sneeze droplets (James Gathany, Public Health Image Library (PHIL)).

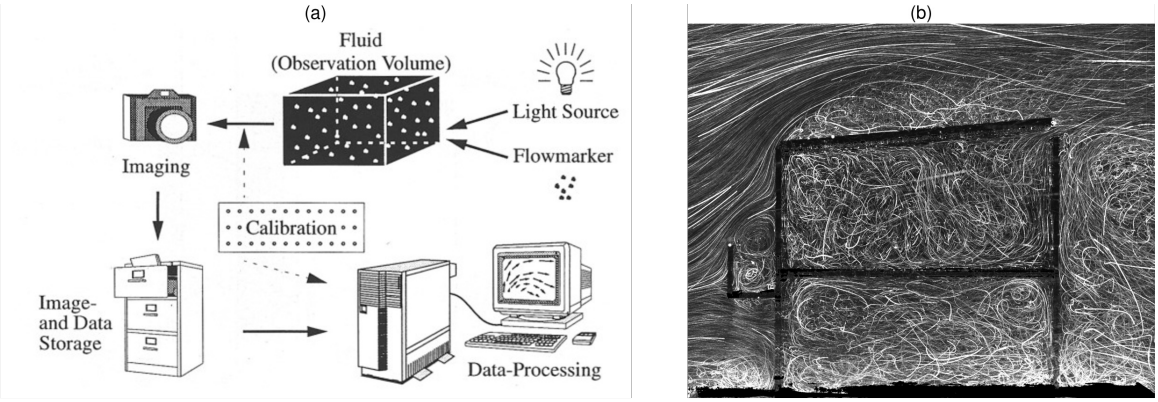


Figure 1.5: (a) PTV setup scheme. Reproduced from [43]. (b) Particle path of outside and inside flows of an Architectural model (Yohsuke Tanaka, Measurement System Laboratory, Kyoto Institute of Technology

multicamera system to reconstruct the three-dimensional particle positions. If the particle density is high, the information obtained from the collective particle motion can be used to obtain the velocity field on a grid as Eulerian information using Particle Image Velocimetry (PIV) algorithms.

In this work, we will describe the experimental setup and the preliminary data obtained using this technique for a high Reynolds turbulent flow generated inside a Von Karman turbine tracking two kinds of particles; the approximately Lagrangian ones and particles with lower inertial effects in order to observe their difference under turbulent flow conditions.

## 1.6 Motivation and outline of the thesis

In this thesis, we analyze the transport of inertial and Lagrangian particles in different flows using a dynamical systems approach. To distinguish the different nature of the problems the thesis has been divided into three parts.

In the first part, we present three papers on the role of transport in the troposphere. In the first paper, we study the transport of water vapor for a well defined atmospheric event; the Atmospheric Rivers. We characterize these events as attracting Lagrangian Coherent Structures (LCS) in the wind field as organizing cores of the transport of water vapor. In the second one, we quantify the mixing in terms of the FTLE and we use it as a potential forecast variable for seasonal prediction over the Atlantic region and the Iberian Peninsula. Finally, in the third one, we study the role of climate sources of mixing variability at a day-scale for the climate period 1979-2014 and for the entire globe.

In the second part, we present three numerical studies where we have addressed the transport in chaotic flows for different kinds of particles. We start by analyzing, the role of the initial conditions for small rigid spheres ($R = const$), where the main forces acting over them are drag and buoyancy. Then, we consider small but non-rigid spheres ($R = R(t)$); bubbles, to study their distribution in the Arnold–Beltrami–Childress (ABC) flow and observe the role of coalescence on path-lines and in particles position distribution. Finally, we analyze the interaction between inertial and Lagrangian particles through a chemical reaction.

In the third part, we focus on experimental trajectories obtained by PTV methods. We

show the preliminary results obtained from a experiment in a von Karman Flow Apparatus in the Göttingen Turbulence Facility 3 (GTF3) at the Max-Planck-Institute for Dynamics and Self-Organization (MPIDS). To explore the smallest scales flow structures of transport, microspheres of 20 $\mu$m has been tracked using a four multi-system high speed cameras into high Reynolds number conditions. Also, we have increased the particle size to 120 $\mu$m to observe the role that smaller inertial effects could have. Nowadays, the experimental results are still under processing, so the experimental setup description and preliminary results are explained to have a first look about the upcoming results.

USC
UNIVERSIDADE
DE SANTIAGO
DE COMPOSTELA

# Chapter 2

# Concepts and tools

## 2.1 Stability and fixed points

The fixed points $\mathbf{r}^*$, solutions of $\dot{\mathbf{r}} = 0$, and introduced in Sec. (1.5) are key to understanding how the particle trajectories are organized.

However, a particle with its initial position slightly different, $\mathbf{r}_\delta = \mathbf{r}^* + \delta\mathbf{r}$, due to a small perturbation $\delta\mathbf{r}$ could have very different behavior depending on the nature of $\mathbf{f}(\mathbf{r})$ around the fixed point. Observing, the dynamics of this perturbation:

$$\dot{\mathbf{r}}_\delta = \frac{d}{dt}(\mathbf{r}^* + \delta\mathbf{r}) = \mathbf{f}(\mathbf{r}^* + \delta\mathbf{r}) = \mathbf{f}(\mathbf{r}_\delta) \tag{2.1}$$

Performing a Taylor expansion of the perturbed point $\mathbf{r}_\delta$ around the fixed point $\mathbf{r}^*$,

$$\mathbf{f}(\mathbf{r}_\delta) = \mathbf{f}(\mathbf{r}^*) + (\mathbf{r}_\delta - \mathbf{r}^*)\left.\frac{d\mathbf{f}}{d\mathbf{r}}\right|_{\mathbf{r}=\mathbf{r}*} + \frac{1}{2}(\mathbf{r}_\delta - \mathbf{r}^*)^2\left.\frac{d^2\mathbf{f}}{d\mathbf{r}^2}\right|_{\mathbf{r}=\mathbf{r}*} \tag{2.2}$$

since $\mathbf{f}(\mathbf{r}^*) = 0$ and neglecting high order terms, then:

$$\dot{\mathbf{r}}_\delta = \delta\mathbf{r}\left.\frac{d\mathbf{f}}{d\mathbf{r}}\right|_{\mathbf{r}=\mathbf{r}*} \tag{2.3}$$

Now, the general solution of the perturbation growth surrounding the fixed point, Eq. (2.3), will be a linear combination of exponential functions and their exponents depend on eigenvalues of $\mathbf{f}$, $(\lambda_1, \lambda_2)$. The motion of ideal particles in incompressible fluid flows is conservative, $\nabla \cdot \mathbf{f} = 0$. If a fluid flow verifies this condition, it means that if there is a contraction in one direction, there should be expansion in the other in the same proportion in order to keep the physical constraint, so the fixed point that verifies this condition is so-called *saddle point*. Since one of the eigenvalues is positive, the saddle is an unstable equilibrium point. Suppose, for example $\lambda_1 < 0 < \lambda_2$ shown in Fig. (2.1). The eigenvalues $\lambda_1$ and $\lambda_2$ are associated with the corresponding eigenvectors $\mathbf{V_1}, \mathbf{V_2}$. The straight lines directed along the eigenvectors $\mathbf{V_1}, \mathbf{V_2}$ are called separatrices. These are asymptotes of other trajectories that have the form of a hyperbola being the reason why the saddle points are also called hyperbolic points. Each of the separatrices can be associated with a certain direction of motion.

If the separatrix is associated with a negative eigenvalue $\lambda_1 < 0$, i.e in our case is directed along the vector $\mathbf{V_1}$, the movement along it occurs towards the fixed point. And conversely, at

$\lambda_2 > 0$ i.e, for the separatrix associated with the vector $\mathbf{V_2}$, the movement is directed from the origin.

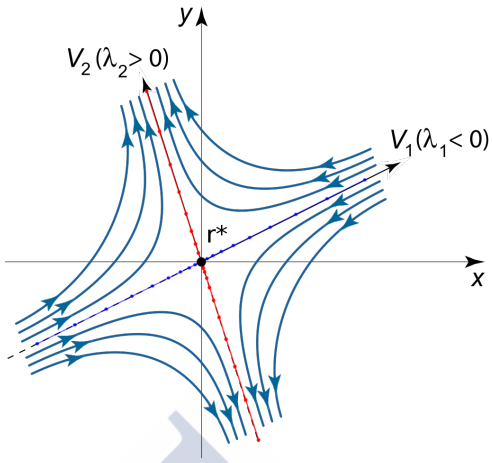


Figure 2.1: Streamlines (light blue) surrounding a saddle point (black dot) and associated invariant manifolds; stable manifold (dark blue) and unstable manifold (red).

In forward time, the trajectories are asymptotic to the $\mathbf{V_2}$ axis; in backward time to the $\mathbf{V_1}$. In this situation, $\mathbf{r}^* = 0$ is called a saddle point, and the $\mathbf{V_1}$ axis is the stable manifold and $\mathbf{V_2}$ axis the unstable manifold.

More formally, we define the stable and manifolds, $M^s$ and $M^u$ , associated with $\mathbf{r}^*$ as follows

$$M^s = \{\mathbf{r} \in \mathbb{R}^n \quad : \quad \mathbf{r} \to \mathbf{r}^* \; as \; t \to \infty\} \tag{2.4}$$

$$M^u = \{\mathbf{r} \in \mathbb{R}^n \quad : \quad \mathbf{r} \to \mathbf{r}^* \; as \; t \to -\infty\} \tag{2.5}$$

Note that a typical trajectory asymptotically approaches the unstable manifold as $t \to \infty$, and approaches to the stable manifold as $t \to -\infty$.

The fixed points and their stable/unstable manifolds act as separatrices partitioning regions of different dynamics. In general, at hyperbolic fixed points, fluid is pulled along the stable manifolds and expelled in diverging directions along the unstable manifolds. Restating, the fixed points are hubs directing the flow and the invariant manifolds delineate how fluid will be directed by those hubs as shown in Fig. (1.2)(a).

This behavior remains relevant in unsteady systems, $\mathbf{f}(\mathbf{r},t)$. However, fixed or periodic trajectories are not commonly encountered in most practical applications due to the general unsteadiness of most flows and the absence of analytical expressions, presenting a big handicap due to implicit time dependence [9]. The role of fixed points is often replaced by appropriately behaved moving trajectories carried by the system as we observe in Fig. (1.2)(b), so the problem of not using a fixed frame to obtain the flow map, increases the difficulty of detection of these points and the associated manifolds.

Trajectories that are hyperbolic at one instant can change their stability at the next instant, so the definition of stable/unstable manifolds turns complex. Also, as we have defined above in Eqs. (**??**), these definitions require the use of asymptotic limits which is unpracticable on real world problems. This is due to the fact that system information comes from finite and discretised

datasets obtained from numerical and/or experimental measures, so trajectories can gain or lose hyperbolicity over time and we are looking to understand inherently transient phenomena.

To estimate this invariant manifolds for real-world problems, the use of other techniques in order to compute the perturbation respect to initial conditions and how it grows and evolves in time requires the use of other approaches as we describe in Sec. (2.4).

## 2.2 Particle motion: Lagrangian and inertial particles

**Lagrangian particles** If we consider a phase point $\mathbf{r}$ just under the influence of time dependent system described by the flow field $\mathbf{v}(\mathbf{r},t)$ the equation of motion is:

$$\frac{d\mathbf{r}}{dt} = \mathbf{v}(\mathbf{r},t). \tag{2.6}$$

As we introduced in Sec. (1.2), this case comes when there are no finite size effects, acting as a point-wise element. There are no forces, so they behave like fluid particles. This condition occurs when density is conserved along the flow as in incompressible fluids, $D\rho_f/Dt = 0$ and the volumes are preserved,

$$\nabla \cdot \mathbf{v} = 0. \tag{2.7}$$

This condition means the absence of sources and sinks in the velocity field and hence the main fixed points are the stagnation points or saddle points.

**Inertial particles** The appearance of finite size effects like density, size, shape, viscosity, etc. Introduce forces and hence accelerations. This increase the dimension of Eq. (2.6), making necessary the evaluate of position and particle velocity, $(\mathbf{r},\mathbf{v}_p)$ to describe its state,

$$\begin{aligned} \dot{\mathbf{r}} &= \mathbf{v}_p \\ \dot{\mathbf{v}}_p &= \mathbf{f}(\mathbf{v}(\mathbf{r},t),\mathbf{v_p},R,\nu,\rho_f,\rho_p,\mathbf{g}...), \end{aligned} \tag{2.8}$$

where $\mathbf{v}_p$ is the velocity of the particle, $\mathbf{v}$ the velocity field of the fluid, $\rho_p$ the density of the particle, $\rho_f$ the density of the fluid, $\nu$ the kinematic viscosity of the fluid, $R$ the radius of the particle and $\mathbf{g}$ the acceleration due to gravity.

Our starting point is the Maxey-Riley-Gatignol equation [44, 45]. It describes the motion of a rigid spherical particle in a non-uniform fluid flow. For simplification from here on, we do not note the function dependences in the equations:

$$\begin{aligned}
\rho_p \dot{\mathbf{v}}_p &= \rho_f \frac{D\mathbf{v}}{Dt} \\
&+ (\rho_p - \rho_f)\mathbf{g} \\
&- \frac{9\nu\rho_f}{2R^2}\left(\mathbf{v}_p - \mathbf{v} - \frac{R^2}{6}\nabla^2\mathbf{v}\right) \\
&- \frac{\rho_f}{2}\left[\dot{\mathbf{v}}_p - \frac{D}{Dt}\left(\mathbf{v} + \frac{R^2}{10}\nabla^2\mathbf{v}\right)\right] \\
&- \frac{9\rho_f}{2R}\sqrt{\frac{\nu}{\pi}}\int_0^t \frac{1}{\sqrt{t-\tau}}\left[\dot{\mathbf{v}}_p(\tau) - \frac{d}{d\tau}\left(\mathbf{v} + \frac{R^2}{6}\nabla^2\mathbf{v}\right)_{\mathbf{r}=\mathbf{r}(\tau)}\right] d\tau
\end{aligned} \tag{2.9}$$

The terms on the right-hand side are the force exerted by the undisturbed flow on the particle, the buoyancy force, the Stokes drag, the added mass correction, and the Basset-Boussinesq history force, respectively. Considering a characteristic length scale $L$, characteristic velocity $U$ and characteristic time scale $T = L/U$, we assume the following restrictions,

$$\begin{aligned}
R(\mathbf{v}_p - \mathbf{v})/\nu &\ll 1 \\
R/L &\ll 1 \\
\left(\frac{R^2}{\nu}\right)\left(\frac{U}{L}\right) &\ll 1.
\end{aligned} \tag{2.10}$$

There is a Stokes flow around the particle, the particle size is very small (in that case, the Faxen corrections, $\nabla^2\mathbf{v} \approx 0$ are negligible) and the factor $R/\sqrt{\nu}$ is also very small. We neglect Basset-Boussinesq history force, as in common practice in the related literature, [46]. We finally rescale space, time and velocity by characteristic scales, $L$, $T$ and $U$, to obtain the simplified equations of motion:

$$\dot{\mathbf{v}}_p = \frac{3\beta}{2}\frac{D\mathbf{v}}{Dt} - \gamma(\mathbf{v}_p - \mathbf{v}) + \left(1 - \frac{3\beta}{2}\right)\mathbf{g} \tag{2.11}$$

with

$$\beta = \frac{2\rho_f}{\rho_f + \rho_p}, \qquad \gamma = \frac{\beta}{St}, \qquad St = \frac{2}{9}\left(\frac{R}{L}\right)^2 Re \tag{2.12}$$

and $t$, $\mathbf{v}_p$,$\mathbf{v}$, and $\mathbf{g}$ now denoting nondimensional variables.

In Eq. (2.13) $St$ denotes the particle Stokes number and $Re = UL/\nu$ is the Reynolds number. The density ratio $\beta$ distinguish neutrally buoyant particles $\beta = 2/3$ from aerosols $(0 < \beta < 2/3)$ and bubbles $(2/3 < \beta < 2)$. The term beginning with $3\beta/2$ represents the added mass effect: an inertial particle brings into motion a certain amount of fluid that is proportional to half

of its mass. For neutrally buoyant particles, the equation of motion is simple, $\frac{D}{Dt}(\mathbf{v}_p - \mathbf{v}) = -\nu(\mathbf{v}_p - \mathbf{v})$.

In this case, $\nabla \cdot \mathbf{f} = Tr(f) \neq 0$, so the dynamics of inertial particles are not conservative and hence the contraction and expansion of the volumes in the phase space will happen even for steady incompressible flow fields.

From the previous equation, other physical parameters can be time-dependent so it could be modeled as an extra dimension on the dynamical system. For example, to describe spherical size changes, $R = R(t)$, like a bubble, the radius should be able to expand and contract [47]. The motion of bubbles in non-uniform incompressible flows was modeled by the momentum equation introduced by [46, 48].

$$\begin{aligned} \rho_p \dot{\mathbf{v}}_p &= \rho_f \frac{D\mathbf{v}}{Dt} \\ &+ (\rho_p - \rho_f)\mathbf{g} \\ &- \frac{9\nu\rho_f}{R^2}(\mathbf{v}_p - \mathbf{v}) \\ &- \rho_f C_L((\mathbf{v}_p - \mathbf{v}) \times \boldsymbol{\omega}) \\ &+ \frac{\rho_f}{2R^3}\left(\frac{d(R^3(\mathbf{v}_p - \mathbf{v}))}{dt} + 2R^3\frac{d(\mathbf{v}_p - \mathbf{v})}{dt}\right) \end{aligned} \tag{2.13}$$

where $\boldsymbol{\omega}$ is the fluid vorticity, $C_L = 0.5$ is the lift coefficient for a sphere. The last two terms are different from Eq. (2.13). The fourth term represents the lift force. The last one, the effect of a spherical bubble with a time dependent-radius $R(t)$, which is modeled by the Rayleigh-Plesset equation [49]:

$$R\ddot{R} + \frac{3}{2}\dot{R}^2 = \frac{P_f - P}{\rho_f} \tag{2.14}$$

where $\dot{R}$ and $\ddot{R}$ are the bubble wall velocity and accelerations respectively. $P_f$ is the pressure at the bubble interface, and $P$ is the pressure field imposed by the flow.

## 2.3 Velocity data: Steady, unsteady and active flows

Here, the flow velocity field $\mathbf{v}(\mathbf{r},t)$ will always be known regardless of the particle nature. It can have multiples origins depending on the problem: analytical flows, numerical simulations; Computer Fluid Dynamics (CFD), hydrodynamic, ocean and weather simulations, and also from experimental results; satellite data or Particle Image Velocimetry (PIV) among others. Real data coming from numerical and experimental results are provided in a discretized way. In this chapter, we will describe the main flows used for the different problems described in the Introduction (Sec. (1.1)).

**Ideal flows** Ideal flows are mathematical functions defined on every point on the space being continuous and differentiable. In general, they are simplified flow descriptions of complex

problems. For example, the ABC flow is the solution of the simplified version of the Euler equation. For other flows, like the double-gyre, the shear flow or the meandering jet, the velocity is expressed as the derivatives of scalar stream functions.

**Atmospheric data** In the case of the wind field, and to address the Lagrangian advection problem on the atmosphere we use discrete velocity fields data provided by the reanalysis database ERA-Interim from ECWMF (European Center for Weather Medium Forecasting) [50]. It is a global atmospheric reanalysis from 1979, continuously updated in real time. The system includes a 4-dimensional variational analysis with a 12-hour window. The full model resolution has a spacing of about $0.703125^\circ$ with a north-south separation which is close to uniform in latitude. There are 128 points aligned along the Greenwich Meridian from the equator to pole. The number of points in the east-west direction varies with latitude, with uniform grid spacing along a particular line. The vertical resolution consists of 60 pressure levels going from the surface up to 0.1 hPa.

**Lagrangian Particle Tracking and Particle Image Velocimetry** Lagrangian Particle Tracking (LPT), also known as Particle Tracking Velocimetry (PTV) is an optical flow visualization technique. It determines the position of particles added to the flow in the three-dimensional space at certain times and assembles these points in trajectories of particles. These trajectories allow the computation of the velocity and the acceleration of the investigated particles. To detect the particles an optical method with digital cameras is used. The LPT method can be separated into three different steps, which will be described individually below. These steps are, first of all, particle finding on each individual image of the cameras, followed by stereo matching of all images taken at the same time - in our case 4 images - and finally connection of the points at different times to trajectories. The information obtained from LPT trajectories can be processed to obtain the velocity field.

In the case that the velocity field consists of discretized data, the integration requires the velocity field to be interpolated in space and time. To that end, higher-order integration and interpolation schemes ensure greater accuracy and smoothness of the computed results, respectively. As we are interested in measuring the trajectory evolution in different flows, and also in quantities derived from the flow, the integration and interpolation schemes are critical in keeping low error results. So both schemes should be chosen with their respective parameters according to the flow and particle conditions. Here, we have used a fourth order Runge-Kutta method with a fixed time step together with a multilinear interpolation. In order to speed up the triangulation of the particles in the interpolation process, the physical coordinates $(\theta, \phi, t)$ have been translated to matrix coordinates using the model resolution. The time step interval was adjusted depending on the problem going from $dt = 0.1$ ms to evaluate the faster process (the bubble contraction and expansion) until $dt = 3$ hours to evaluate the Lagrangian transport on the atmosphere. On the Lagrangian transport, where irreversible process are not involved, to check the accumulated errors, an integration of uniform grids of particles has been done in forward integration from a time $t_0$ to a time $t_0 + T$ and then a backward integration was done, reversing the time till $t_0$ using different $dt$, to observe the difference between the initial grid positions and the final one. The error due to integration/interpolation tandem was considered lower if the accumulated error between all the particles was lower than 5%.

## 2.4 Lagrangian Methods

### 2.4.1 Lagrangian Coherent Structures

As complexity of fluid flows increases, the motivation to identify hyperbolic fixed points and invariant manifolds for aperiodic flows, becomes compelling. However, fixed or periodic trajectories are not commonly encountered in most practical applications due to the general unsteadiness of most flows. Applying the invariant manifolds theory in temporally aperiodic flows is a challenge [51, 52, 53] due to the absence of fixed points and hyperbolicity can change their stability (not a problem for steady systems) from one instant to another. Moreover, the definitions of stable/unstable manifolds require asymptotic limits [54] as we defined on Sec. (2.1), which struggle with "real world" data.

The invariant manifolds for systems with general time dependence have fallen under the broader category of Lagrangian Coherent Structures [11]. This categorization extends the concepts and methodologies of stable and unstable manifolds of steady systems for time-dependent systems. It provides a more precise and (temporally relevant) depiction of common fluid mechanics constructs (e.g, eddies, flow separation, and stirring) controlling the stretching, folding and alignment mechanism underlying kinematic mixing. These structures act as separatrices of different dynamical regions on the flow delimited by boundaries separating regions of coherent dynamics, given a similar phase portrait or flow topology in the same way that stable/unstable manifolds do [55, 56]. Due to their separatrix behavior, Haller [57] defines these structures, in a broad sense, as the locally strongest repelling or attracting material surfaces (surfaces of particles).

The Lagrangian Coherent structures have the main following properties:

- They are frame independent. They must be independent of coordinate changes. The deformation itself over its neighborhood guarantees that the LCS cannot depend on the frame chosen as any other Eulerian quantity does. For example, the Okubo-Weiss parameter [58, 59] depends on the point of view from where the data has been taken. Thus, for example, someone transported in an eddy does not have the same perception that someone who observes the eddy from outside does.

- They can be computed in forward and backward time directions. Attracting LCS are analogously computed by reversing time, as expansion in backward time implies contraction in forward time. In the same way that for steady systems, the stable and unstable manifolds can be understood in a forward and backward sense regarding the approximation or moving away from the fixed point.

- The structures are termed Lagrangian because they are defined from the fluid motion, as opposed to an instantaneous Eulerian snapshot, and they are themselves material surfaces advected by the flow. The flow shapes the material continuum surfaces approximated in a discretized way by a tracers grid. This deformation propagates under the flow influence.

- They are material lines (lines of particles). There is no net flux across them acting as transport barriers shaping the tracers patterns. Comparing to steady analytical flow fields and the asymptotic streamlines, the invariant manifolds ensures that there is no net flux towards the invariant manifolds acting as separatrices of different dynamical regions.

- They are also termed coherent because they have distinguished stability compared to nearby material surfaces and, consequentially, LCS can often be identified with familiar flow features.

To detect such manifolds we will use the concept of hyperbolicity in an indirect way. Instead of testing different surfaces to measure the expansion and contraction around it, we will use an approach based on the distribution of Finite-Time Lyapunov Exponents (FTLEs), which will be introduced below. We discretize the fluid domain with a dense grid of material points, measure the Lagrangian expansion rate (roughly "hyperbolicity") about each material point, plot the spatial distribution, and extract surfaces that maximize the measure [**?** ]. This approach allows us to understand better the nature of the fluid, however, this notion of hyperbolicity opposite to steady systems must be associated to a specific time interval which is typical of finite-time analysis, so this behavior will depend on our "horizon of knowledge".

This approach is different with respect to the one used for steady systems where the invariants are obtained based on linearized systems around the fixed point. It seeks to be independent of any specific hyperbolic trajectory, whereby the distribution of an appropriate hyperbolicity measure generally reveals all influential finite time hyperbolic structures (e.g. the relevant hyperbolic trajectories and their associated stable and unstable manifolds).

The attracting LCS will generally be distinguishable from advection of material points since the fluid is attracted to and along these surfaces. In general, repelling LCS are hidden from flow visualization, despite playing a fundamental role in transport. The computation of attracting and repelling LCS allow us to go further in the understanding of coherent structures in the fluid flow, revealing unhidden and showing the surfaces that constitute the coherent structures that organize the fluid flow transport.

In conclusion, Lagrangian-based measures that explicitly track the fluid motion are less common, and in many cases ad hoc or qualitative and succinctly encode key Lagrangian information into a single field from which we can define structures that remain relevant in space and time, are coordinate-frame invariant and perhaps most importantly convey information regarding fundamental mechanics of fluid transport. The LCS computation proceeds regardless of the time dependence, making it applicable in more general settings. Together, these LCSs reveal highly relevant information that is notably absent when employing traditional analysis techniques (e.g. velocity field, vorticity, streamlines, and Q-criterion [60]).

### 2.4.2 Finite-Time Lyapunov exponents (FTLE)

In fluid mechanics, hyperbolicity is often synonymous with its manifestation, of stretching. In a broad sense, a trajectory is hyperbolic if infinitesimal perturbations to that trajectory expand or contract over time. However, this is not global interpretation mainly due to the fact that this behavior can change over time, and long-term limits cannot be computed. This interpretation makes suitable the use of the FTLE (Finite Time Lyapunov Exponent) as a measure of finite-time hyperbolicity. We focus on the FTLE because it has been most widely used, and more results exist for this method [57, 61, 62, 63].

Lyapunov exponents, in general, have long been used to determine the predictability or sensitivity to initial conditions in dynamical systems. They measure the exponential growth rate of separation between initially close trajectories separated by a distance $d$ for $t \to \infty$,

$$\mu = \lim_{t\to\infty} \frac{1}{t} \ln\left(\frac{d_f}{d}\right), \tag{2.15}$$

where $d_f$ is the final separation when $t \to \infty$.

Due to the "real word" limitations mentioned, the use of long term limits $t \to \infty$ is not feasible, so a finite time version is required. Following the same procedure as in Sec. (2.1) for a particle state at a time $t_0$, $\mathbf{r}(t_0) = \mathbf{r}_0$ and a perturbed state $\mathbf{r}_{\delta 0} = \mathbf{r}_0 + \delta\mathbf{r}_0$ by a distance $\delta\mathbf{r}_0$, both, under the flow map action taking a particle at $\mathbf{r}_0$ and transporting it, after a time $T$ to $\mathbf{r} = \phi_{t_0}^{t_0+T}(\mathbf{r}_0)$, the linearized perturbation growth surrounding $\mathbf{r}_0$ is,

$$\delta\mathbf{r}(t_0+T) = \phi_{t_0}^{t_0+T}(\mathbf{r}_\delta) - \phi_{t_0}^{t_0+T}(\mathbf{r}) = \frac{d\phi_{t_0}^{t_0+T}(\mathbf{r})}{d\mathbf{r}}\delta\mathbf{r}(t_0) + O(\| \delta\mathbf{r}(t_0) \|^2)). \tag{2.16}$$

Neglecting the term $O(\delta^2)$ and measuring the norm of the perturbation $\delta\mathbf{r}(t_0+T)$,

$$\begin{aligned}\|\delta\mathbf{r}(t_0+T)\| = \sqrt{\left\langle \frac{d\phi_{t_0}^{t_0+T}(\mathbf{r})}{d\mathbf{r}}\delta\mathbf{r}(t_0), \frac{d\phi_{t_0}^{t_0+T}(\mathbf{r})}{d\mathbf{r}}\delta\mathbf{r}(t_0)\right\rangle} = \\ \sqrt{\left\langle \delta\mathbf{r}(t_0), \frac{d\phi_{t_0}^{t_0+T}(\mathbf{r})}{d\mathbf{r}}^H \frac{d\phi_{t_0}^{t_0+T}(\mathbf{r})}{d\mathbf{r}}\delta\mathbf{r}(t_0)\right\rangle} = \sqrt{\langle \delta\mathbf{r}(t_0), \mathbf{G}\delta\mathbf{r}(t_0)\rangle},\end{aligned} \tag{2.17}$$

where $\mathbf{G}$ is the finite-time version of the (right) Cauchy-Green deformation tensor,

$$\mathbf{G} = \nabla\phi_{t_0}^{t_0+T}(\mathbf{r})\nabla\phi_{t_0}^{t_0+T}(\mathbf{r})^H = \mathbf{F}\mathbf{F}^H \tag{2.18}$$

being $\mathbf{F}$ the gradient of the flowmap. $H$ denotes the adjoint of the matrix, being the transpose for a symmetric matrix.

The maximum stretching between $\mathbf{r}_\delta$ and $\mathbf{r}$ happens when $\delta\mathbf{r}(t_0)$ is aligned with the eigenvector associated with the maximum eigenvalue of $\mathbf{G}$, $\mu_{max}$. Then,

$$\max_{\delta\mathbf{r}(t_0)} \|\delta\mathbf{r}(t_0+T)\| = \sqrt{\left\langle \overline{\delta\mathbf{r}}(t_0), \mu_{max}(\mathbf{G})\overline{\delta\mathbf{r}}(t_0)\right\rangle} = \sqrt{\mu_{max}}\left\|\overline{\delta\mathbf{r}}(t_0)\right\| \tag{2.19}$$

The asymptotic limits defined in Eq. (2.15) turn into,

$$\begin{aligned}\lim_{t\to\infty} &\approx t \to T \\ \frac{d_f}{d_0} &\approx \frac{\|\delta\mathbf{r}(t_0+T)\|}{\left\|\overline{\delta\mathbf{r}}(t_0)\right\|} = \sqrt{\mu_{max}},\end{aligned} \tag{2.20}$$

and the Finite Time version of the Lyapunov Exponent (FTLE) is

$$\sigma_{t_0}^T = \frac{1}{T}\ln\sqrt{\mu_{max}(\mathbf{G})}. \tag{2.21}$$

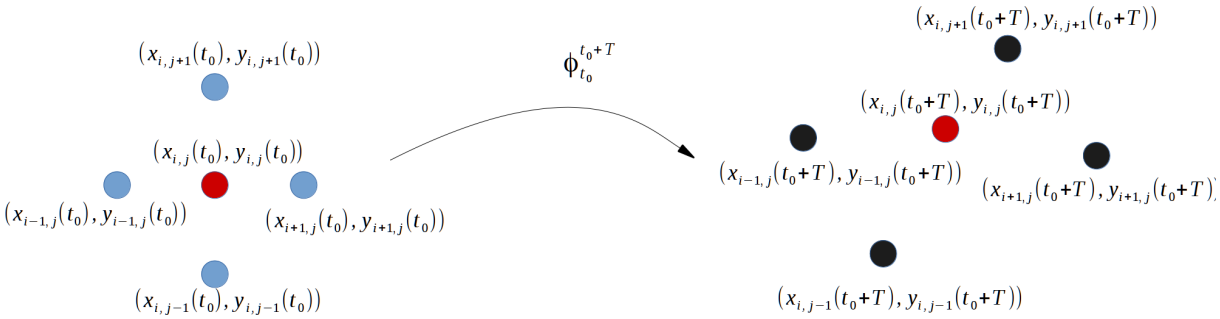


Figure 2.2: Scheme of numerical derivative of the flow map gradient. Modified from [64]

The largest FTLE $\mu_{max} = \mu_1$ is often referred to without distinction as the FTLE. The eigenvector associated to the largest eigenvalues will eventually dominate the perturbation growth of that component. This can be considered as spherical deformation regarding a material element where the sphere will be deformed into an ellipsoid due to the action of motion. The major axis of this ellipsoid will coincide with the eigenvector associated to the maximum eigenvalue. In the same way, the minor axis will coincide with the lower eigenvector associated to the minimum eigenvalue. For volume-preserving flows, the sum of Lyapunov exponents must be zero.

The $\sigma$ field in Eq. (2.21), measures the exponential growth rate of a small perturbation for a given finite time $T$. The FTLE field can be computed in forward and in backward time directions, thus, maximal regions of FTLE are characterized by a perturbation growth faster than the surrounding flow allowing us to estimate the LCSs

**Numerical computation** The standard method to compute the FTLE field is schematized in Fig.(2.2). It starts with the initialization of a grid of material points equally spaced in a structured grid at $\mathbf{r}_{0ij}$ time $t_0$. This simplifies gradient computation and does not require a priory knowledge of the flow topology, which makes the discussion most broadly applicable [9, 62]. The initial locations of these points, as opposed to the final locations, represent the locations at which FTLE will be computed – the FTLE grid. Then, we solve the trajectory equation, Eq. (1.12) for each material point for a finite time interval, $[t_0, t_0+T]$, and to compute the numerical gradient of the flow map in Eq. (2.18), we use second order accurate central differences in the interior points and first order (forward or backwards) differences at the boundaries as shown in Eq. (2.22).

In Cartesian coordinates and for a two-dimensional problem, $\mathbf{r} = (x, y) \in \mathbb{R}^2$, the numerical gradient is:

$$\mathbf{F} = \left.\frac{d\phi_t^{t_0+T}(\mathbf{r})}{d\mathbf{r_0}}\right|_{\mathbf{r}_{i,j}} = \begin{bmatrix} \dfrac{x_{i+1,j}(t_0+T) - x_{i-1,j}(t_0+T)}{x_{i+1,j}(t_0) - x_{i-1,j}(t_0)} & \dfrac{x_{i,j+1}(t_0+T) - x_{i,j-1}(t_0+T)}{y_{i,j+1}(t_0) - y_{i,j-1}(t_0)} \\ \dfrac{y_{i+1,j}(t_0+T) - y_{i-1,j}(t_0+T)}{x_{i+1,j}(t_0) - x_{i-1,j}(t_0)} & \dfrac{y_{i,j+1}(t_0+T) - y_{i,j-1}(t_0+T)}{y_{i,j+1}(t_0) - y_{i,j-1}(t_0)} \end{bmatrix}. \tag{2.22}$$

For spherical coordinates fields $\mathbf{r}(\theta, \phi)$ in a longitude-latitude mesh (Sec. (1.5.1)), we require the spherical correction $\mathbf{S}$ for (2.18), $\mathbf{G} = \mathbf{F} \times \mathbf{S} \times \mathbf{F}^T$, defined in [65] as:

$$\mathbf{G}(\mathbf{r})_{i,j} = \begin{bmatrix} \dfrac{\theta_{i+1,j}(t_0+T)-\theta_{i-1,j}(t_0+T)}{\theta_{i+1,j}(t_0)-\theta_{i-1,j}(t_0)} & \dfrac{\theta_{i,j+1}(t_0+T)-\theta_{i,j-1}(t_0+T)}{\phi_{i,j+1}(t_0)-\phi_{i,j-1}(t_0)} \\ \dfrac{\phi_{i+1,j}(t_0+T)-\phi_{i-1,j}(t_0+T)}{\theta_{i+1,j}(t_0)-\theta_{i-1,j}(t_0)} & \dfrac{\phi_{i,j+1}(t_0+T)-\phi_{i,j-1}(t_0+T)}{\phi_{i,j+1}(t_0)-\phi_{i,j-1}(t_0)} \end{bmatrix} \times \begin{bmatrix} R_T^2 \sin^2(\theta_{i,j}(t_0+T)) & 0 \\ 0 & R_T^2 \end{bmatrix} \times \begin{bmatrix} \dfrac{\theta_{i+1,j}(t_0+T)-\theta_{i-1,j}(t_0+T)}{\theta_{i+1,j}(t_0)-\theta_{i-1,j}(t_0)} & \dfrac{\phi_{i,j+1}(t_0+T)-\phi_{i,j-1}(t_0+T)}{\phi_{i,j+1}(t_0)-\phi_{i,j-1}(t_0)} \\ \dfrac{\phi_{i+1,j}(t_0+T)-\phi_{i-1,j}(t_0+T)}{\theta_{i+1,j}(t_0)-\theta_{i-1,j}(t_0)} & \dfrac{\theta_{i,j+1}(t_0+T)-\theta_{i,j-1}(t_0+T)}{\phi_{i,j+1}(t_0)-\phi_{i,j-1}(t_0)} \end{bmatrix}. \quad (2.23)$$

This approach is highly flexible, allowing for variations in the distribution and resolution of trajectory information, which can ultimately influence the accuracy and performance of LCS identification.

**LCS as ridges in the FTLE field** In this work, we focus on the detection of LCS based on the FTLE ridge extraction introduced by Shadden et al. [62]. A ridge of FTLE is essentially a curve where it is locally maximized in the transverse direction, leading to a "second-derivative ridge" definition that required that a ridge was a curve (more generally, hypersurface in high dimensions), requiring the following conditions:

1. The first derivative of the FTLE field (Eq. (2.21)) must be zero in the normal direction $\mathbf{n}$,

$$\mathbf{n} \cdot \nabla \sigma = 0. \quad (2.24)$$

2. The second derivative of the field must be negative and minimum in the normal direction,

$$\varepsilon_{min}(\nabla^2 \sigma) < 0, \quad (2.25)$$

   where $\varepsilon_{min}(\nabla^2\sigma)$ is the minimum eigenvalue of $\nabla^2\sigma$.

3. The largest Lyapunov exponent $\mu_{max} = \mu_1$ must be positive. There should be attraction within the surface and repulsion normal to it,

$$\mu_1 > 0 > \mu_2 \quad (2.26)$$

**Integration time and domain boundaries** The selection of the finite integration time $T$ is arbitrary and should be preselected depending on the phenomena. It should be long enough to allow dominant flow features to have a chance to emerge, to let the particle grid "suffer" the deformation gradient, but no so long that the final positions used to compute the deformation

gradient are uncorrelated to the flow features we are trying to expose back at the initial time when the material points were released. Some effort has been made to determine it [66] or at least to define a lower boundary [57]. Main problems manifest when some ridges can only be observed within a particular time window, showing different behaviors depending on $T$. Also, the observation of segmented LCS, is due to some points revisiting the same region or due to lower resolution grid velocity field which are not solving correctly lower feature scales. Also, the appearance of other secondary structures can obscure and disturb the interpretation of the FTLE. LCS can show variability over time, they can grow, appear or disappear with changes in the integration time. For long-time and robust LCS, the variations on the FTLE are gradually increased tending to sharpen along the LCS due to the influence of the hyperbolic regions on the domain. Most of the FTLE sensitiveness happens at short times where the LCS is not well defined. From the practical view, when the velocity data is finite, the boundary problem domain should be taken into account, due to the integration of trajectories not being able to proceed beyond the time interval or domain boundaries. Tang et al. [16] proposed the use of linearized information to extrapolate the fluid flow to keep a linear separation homogeneous rate outside the domain, while other points can remain inside longer times. To summarize, the integration time is usually determined by grid spacing (computational cost), the time scale of the dynamics, and/or availability of data.

### 2.4.3 Drawbacks of the FTLE

This methodology to obtain the FTLE and LCS is already matured and some deficiencies were noted. As we described above, the FTLE is derived from the largest eigenvalue of the finite-time strain tensor, however, the information encoded here is not complete due to the fact that the FTLE does not take into account how the deformation happens. This is important depending on the type of study and how rigorous the definition of the LCS can be. Stable/unstable manifolds do not always produce ridges in the FTLE field [11, 62, 67], or despite being separatrices they are not necessarily the most repelling or attracting surfaces. This has mainly been demonstrated in simple flows, as noted in [67]. For example, a shear flow [61, 57], will produce high FTLE values however there is no "hyperbolic" trajectories growth, it being linear. In the case that we want to be more rigorous and obtain those surfaces that are normally hyperbolic and ensure that LCS is locally the most normally repelling surface, a refinement of the FTLE ridge definition should be made. Haller [57] derived necessary and sufficient conditions for LCS in terms of invariants of the strain tensor to ensure that the direction of dominant expansion/contraction converges to the normal direction.

Some results [68] show that most of the structures are normally hyperbolic, and in general this deformation grows exponentially in time while the shear deformation makes it linear. One might expect, that for sufficient integration time, the hyperbolic structures are remarked in comparison with shear structures when plotting FTLE, however, this approach is not straightforward due to any type of growth in finite time will have an associated exponent. Despite mathematical rigorousness, LCS are physical objects and they are present in the flow and will exist independent of any method employed to measure LCS. FTLE can be considered as "less rigorous" than others, but it provides a good first approach to explore the LCS and/or separatrices in fluid flows.

### 2.4.4 Other approaches for LCS detection

The search for mathematically rigorous definitions of LCS continues. Beron-Vera et al. [15] analyzed the different types of structures that are possible, different from normally hyperbolic. The combination of shear and hyperbolic expansions or in other words, tangential and normal deformation will be present in most practical applications and both can change over time and space, so the formulation of a general theory to distinguish perfectly both deformation and classify these structures is still in progress.

Haller [69] presents a review of the techniques, providing the complete foliation of the material surfaces and also detecting other material deformation related with coherent structures such as elliptical LCS or parabolic LCS.

The methods presented in this review [69] are a continuation from the variational methods started in [57] regarding variational principle. The key of variational methods is to find functions which extremize the value of quantities that depend upon those functions. Here, instead of searching for functions in the pure sense, we seek for material surfaces that maximize a certain type of deformation in the finite time interval of interest. In the case of hyperbolic LCS detection, there are two approaches; a local and global one. The main difference between both is that the local one uses the local deformation associated to a line or set of initial conditions through its normal and tangential components. The global variational approach uses the averaged information over a set of lines to find those ones without a particular deformation (shearless or strainless LCS if we are interested in elliptic LCS).

Elliptic LCSs are closed and nested material surfaces that act as building blocks for the Lagrangian equivalents of vortices, they are mainly rotation-dominated regions of trajectories that generally traverse the phase space without substantial stretching or folding. In general, the methods focusing on the rotational component of the deformation, observe how the tangent vectors to trajectories rotates. For example, the rotational coherence from the Polar Rotation Angle (PRA) [70] measures the angle between the eigenvectors associated to the rotation deformation. Another method, [71], the Lagrangian-Averaged Vorticity Deviation (LAVD), measures how intense the anomaly of the vorticity is along its trajectory, so high values of the integrated anomaly show elliptic dominated regions as eddy cores.

A review of the most used LCS detection methods with their advantages and disadvantages have been recently published [72].

USC
UNIVERSIDADE
DE SANTIAGO
DE COMPOSTELA

# Chapter 3

# Lagrangian transport in the atmosphere

## 3.1 Main goals

One of the problems addressed in this thesis is the study of Lagrangian trajectories of fluid points in the atmosphere. Here, we have used real aperiodic data obtained from ECWMF atmospheric reanalysis model [50] described in section (2.3).

The atmosphere is well known to be a complex problem due to its turbulent behavior with a continuous spatiotemporal scale and nonlinear coupling through their scales of motion. Despite its complexity, persistent coherent and finite amplitude flow features are also observed and their role in transport and mixing will be addressed here. We will focus on the deformation of Lagrangian tracer patterns due to wind field, using some simplifications and spherical corrections for the equations of motion and the FTLE computation.

However, beforehand, the use of Lagrangian analysis to study the atmosphere has some drawbacks: the error accumulated due to numerical integration in the atmosphere grows exponentially in time mainly due to the unresolved processes and scales of motion constraining the integration limits.

Thus, the Lagrangian approach of transport for the whole atmosphere for all spatiotemporal scales is an overwhelming problem. All these handicaps require simplifications and focusing on particular scales to make it affordable: the use of 2D pressure layers focusing on horizontal transport, consideration of the flow as incompressible, neglection of the vertical deformation, short finite time advection less than two weeks, or the use of passive fluid particles to follow the path-line due to bulk motion of air masses, are some of the simplifications performed throughout this chapter.

Also, it requires reducing each structure individually to make an identification analysis to observe its role from a Lagrangian point of view. Here, in this section, we address this issue partially, considering a predefined timescale in order to study the transport at the mesoscale, focusing in the troposphere where most of the atmospheric phenomena take place.

We pay attention to one kind of coherent structure on the troposphere, the so-called Atmospheric Rivers. This meteorological phenomenon is a wind jet shape propagating from lower to medium latitudes, carrying high amounts of water vapor and latent heat, being a key mechanism to redistribute the heat over the globe. Its length is higher than 2000 km and a width less than 500 km with a life of a week. Their jet strain shape together with their stability make them suitable to be studied in terms of dynamical systems and Lagrangian Coherent Structures.

In this section, we present three articles where the tools and the concepts explained in the

previous chapters have been applied to the mentioned problem.

## 3.2 Lagrangian Coherent Structures Along Atmospheric Rivers.

In the first paper, we focus on the Atmospheric Rivers described above. Our goal has been to identify this troposphere transport phenomenon as a Lagrangian Coherent Structure (LCS). To that end, we focus on ten AR selected events over the Atlantic Ocean with a live-time of days in different seasons. We use three different approaches of a representative vector field $\mathbf{v}(\mathbf{r},t)$ for ARs. First, we have considered a two-dimensional model of the troposphere using the integrated water vapor flux weighted by the amount of water vapor to obtain a velocity field which enhances the AR jet region where the vapor is mainly transported. Second, we have considered a two-dimensional wind velocity field at different pressure levels, slicing the troposphere from 1000 hPa to 750 hPa. Third, we have performed a case study using the three-dimensional wind field, to check qualitatively the two-dimensional models previously defined and the coherence of the horizontal transport. We have computed the FTLE field in forward and backward time direction using a time integration of 5 days. Then, we have performed a LCS analysis based on ridge extraction from the FTLE field for two-dimensional cases. For the three-dimensional case, the LCS has been estimated using the isosurfaces of the FTLE field. In addition, we compare the reliability of Lagrangian tracers with water vapor particles. We also compare the patterns of tracer field advected by two AR events; one with a clear jet shape dominated by passive advection and another mainly dominated by evaporation.

Our results conclude that for winter ARs mainly dominated by a passive advection, there is an attracting LCS along the AR, compressing the water vapor while it moves towards east. For an AR with a clear jet shape structure, the LCS keeps its spatial coherence in the vertical direction shown as a curtain in 3D.

The full content of the article can be consulted on `https://aip.scitation.org/doi/full/10.1063/1.4919768`

## 3.3 Influence of finite-time Lyapunov exponents on winter precipitation over the Iberian Peninsula.

In the second article, we have used the FTLE statistics as a measure of mixing over the North Atlantic region to explore its usability as a forecast variable for months in advance. Using the wind field at 850 hPa, we have performed Lagrangian simulations to obtain the forward FTLE time series within a 5 day time integration for a climate period of 35 years. Then, the monthly-average anomaly of FTLE has been computed to estimate the mixing over the Atlantic Region. It has been correlated with the precipitation over the Iberian Peninsula, finding a high correlation with the precipitation in the following season. Also, to understand the meteorological mechanism behind this correlation, the same procedure has been applied to different Climate Indexes and other meteorological variables, in agreement with the previous results obtained.

The full content of the article can be consulted on `https://www.nonlin-processes-geophys.net/24/227/2017/`

## 3.4 Climatology of Lyapunov exponents: The link between atmospheric rivers and large-scale mixing variability

In the third article, we study the mixing at day-scale in the troposphere over the entire globe in terms of FTLE. We have analyzed different sources of mixing and its variability through a climate analysis. Following the same procedure as in previous articles, we have computed in forward and backward time direction the FTLE time series for the climate period 1979-2014 for the entire globe. In other terms, we have obtained the evolution of the deformation of air masses at a day-scale to estimate the tropospheric mixing for the climate period mentioned above. We have also studied the role that climate sources of variability, like seasonality or ENSO events play on mixing, through an analysis of intranual and interannual variability of FTLE time series. In addition, two sources of tropospheric mixing have been considered; first, the baroclinicity through the Eady Growth Rate as a trigger mechanism on the formation of flow structures. Second, we have considered the ARs activity over the Atlantic region, filtering the FTLE time series with an AR detection database to quantify their influence in terms of mixing. To support this, we compare the precipitation in the Sahara region and the UK. We found that mixing calculated over statistics of FTLE time series reproduces well the main climate patterns and also the main variability climate sources. The forward FTLE intrannual variability shows the influence the pressure centers have, on the mixing over the northern and southern hemisphere. The backward FTLE intraanual variability has its better agreement with the ITZC area. The interannual variability of the time series shows its strongest signal over the Pacific Warm Pool where the El Niño and La Niña events, are the main sources of variability. This fact has been further studied, analyzing the annual time series of MEI (Multi ENSO Index) and the anomaly of the FTLE for the defined region obtaining high correlation values in agreement with the previous results.

The full content of the article can be consulted on `https://www.earth-syst-dynam.net/8/865/2017/`

## 3.5 Conclusions

The FTLE provide a versatile tool to analyze Lagrangian transport in the atmosphere. Focusing on a particular event, it allows us to characterize the wind flow structures as LCS, giving us quantitative information about the different dynamical regions on the wind field. Here, we have found that ARs dominated by strong winds and passive advection behave as attracting LCSs, over the Atlantic Ocean shaping the water vapor patterns. Its activity together with other tropospheric flow structures introduces mixing in the troposphere and hence displaces the air masses, conditioning the regional weather. The use of statistical analysis is essential to summarize the mixing over the years and over the region in question. We found that the statistic based on FTLE fields can be used as a forecast variable over the North Atlantic area; the link between mixing and precipitation some months in advance over the Iberian Peninsula shows an agreement in terms of meteorological variables and different climatic indexes. The use of the FTLEs over the entire globe provides a climate description in terms of mixing at a day scale, reproducing in a climate sense, the same patterns as other meteorological variables. The main sources of climate variability, seasonal change and ENSO, have been reproduced, showing the role that they have in mixing at the mesoscale. Also, the link between baroclinic instability and

mixing at day scale has been computed in average climatic terms, supporting that those regions with instability coincide with regions of high mixing.

Finally, once a coherent structure like the ARs has been identified as a maximal FTLE region, we filter the associated time series in terms of dynamical structures, distinguishing their contribution to the mixing.

The FTLE, as an integrated Lagrangian measure, allows us to explore geophysical flow structures in terms of mixing. To go further in this analysis, more accurate computations could be done: for example, the use of more accurate LCS extraction methods, an extended three-dimensional analysis to other atmospheric events, and/or the use of other advection times $T$ to explore the role of other flow structures and quantify their contribution to mixing. The methodology used here can be extended to other regions and other atmospheric levels.

USC
UNIVERSIDADE
DE SANTIAGO
DE COMPOSTELA

# Chapter 4

# Transport of inertial particles in chaotic flows

## 4.1 Main objetives

For Lagrangian tracers, the time-position vector state is enough to describe the phase map. However, when we introduce finite size effects to study problems where realistic particles are involved, the presence of forces and the local flow velocity drive the motion of inertial particles. Accelerations are required to describe the state of a particle increasing its complexity with respect to the Lagrangian problem, allowing the particles to overcome the flow constraint and hence the transport barriers for Lagrangian particles. This makes the problem exponentially expensive in computational cost and hence making it more difficult to detect separatrices and invariant manifolds due to the heavy requirements needed to evaluate the whole phase space of initial conditions to obtain the FTLE fields.

Many studies have been done on the dynamics of inertial particles in model flows to observe their effects on collective motion and distribution as we introduced in Sec. (1.5.2). The sensitive dependence on the initial conditions of inertial particle trajectories and clustering was further studied by [73] using a two-dimensional cellular flow for neutrally buoyant particles. A method to segregate inertial particles from an initial mixture by different sizes (i.e. Stokes numbers) was numerically demonstrated in [74].

In this section, we will mainly focus on the simplified form of the Maxey-Riley equation described in Sec. (2.2). We focus on how the inertial effects modify particle trajectories and other physical properties relative to their collective motion on different model flows and compare it with the Lagrangian tracers for three different kinds of particles; rigid spherical, non-rigid spherical (bubbles) and reactive particles. To that end, we perform particle parameter variation on Eq. (2.12) like the radius, density relation and also the modification of the initial conditions; position and initial velocity [75].

To quantify the sensitiveness to these parameters, we use the FTLE field to obtain the separatrices that organized the motion of particles with a different dynamic, however, the gradient of the flow map on Eq. (2.18), should be extended to take into account the additional dimensions. In higher dimensional problems, the computation of this matrix is an overwhelming task so we should focus on a section of the subspace, which can be considered "slices" of the full problem. The dimensional slices will depend on which dimensions we would like to study the sensitivity of. Here, for those highly dimensional problems, we will focus on how these

perturbations grow in the *xy* plane by integrating the particle trajectories numerically, from which the sensitivity field is computed.

Also, for time-dependent vector fields, the location of these separatrices depends on the choice of initial time, so the locations of ridges depend also on it. In this section, we will not perform a time variation analysis to measure the change of the FTLE and LCS patterns to observe its evolution. We will focus on periodic and steady flows.

In this section, we present three articles where the tools and the concepts explained above have been applied to the problem mentioned.

## 4.2 A method to calculate finite-time Lyapunov exponents for inertial particles in incompressible flows.

In the first paper, we have studied the influence that initial velocity conditions have on the trajectories for small rigid spherical particles, splitting the space sensitivity from velocity sensitivity for two model flows considered; the meandering jet and the double-gyre. The evolution of a perturbation is along four basis vectors. For an arbitrarily oriented initial perturbation, the growth may not be dominated in the direction of greatest expansion for short integration times. This can be overcome by sampling multiple perturbations in different directions. We have considered a finite range of initial conditions $\mathbf{r}_0 \in \mathbb{R}^4$ in the range of flow characteristic scales, to focus on a four-dimensional region of the phase space. After the integration, we have computed the FTLE using a four-dimensional deformation gradient tensor, including the deformation of velocity and position with respect to the initial conditions, so each tensor difference point has eight neighboring points, one along each of the positive and negative directions in each phase space direction. The deformation is measured with respect to the perturbation of the initial state conditions of the system, providing a unique value; the maximum deformation, without knowing its main direction. We should focus on the information contained on the eigenvectors and the main stretch direction to observe the dimension where the maximum stretching happens and observe, how relevant it is respect to characteristic scales of the flow. This allows us to identify the causes of deformation; perturbations on initial position or velocity. Also, this situation has been tested with heavy and light particles to observe its reliability to obtain the flow partitions.

The full content of the article can be consulted on `https://www.nonlin-processes-geophys.net/22/571/2015/`

## 4.3 Mixing of spherical bubbles with time-dependent radius in incompressible flows.

In the second paper, we have focused on non-rigid spherical particles: spherical bubbles. The dimensionality increases to include the radius and its rate of change $R(t), dR(t)/dt$ as state variables. We have used the steady three-dimensional ABC flow with a gradient of pressure and temperature on the $z$ axis allowing the contraction and expansion of bubbles, modeled by the Rayleigh-Plesset equation and the equation of state, turning into an 8-dimensional problem. However, due to its high dimensionality, we focus on a section of the subspace $(x, y)$ to observe the influence that initial radius $R_0 = R(t_0)$ conditions have on the particle trajectories in terms of FTLE spatial distribution comparing it with Lagrangian distribution. In addition, the effect of coalescence has been considered by means of a geometrical approach to solve the collision between bubbles, considering a different distribution of initial bubbles controlled by the initial radius and the initial distance between the bubbles $d_0$. This effect has been assessed obtaining collision rates and it has been studied in terms of Levy distributions.

The full content of the article can be consulted on `https://journals.aps.org/pre/abstract/10.1103/PhysRevE.93.023107`

## 4.4 Nonperfect mixing affects synchronization on a large number of chemical oscillators immersed in a chemically active time-dependent chaotic flow.

Finally, in this paper, we have studied the problem of mixing/dispersion of chemically active particles through a Belousov-Zhabotinsky reaction, where mixing is not well realized. To that end, the chemical reaction is modeled by a large population of Lagrangian particles (a chemical dissolved in solution) and inertial particles (catalyst-loaded beads) moving in a double-gyre flow. The chemical reaction between both particles has been modeled using a three variable Oregonator model. The dynamics of the system have been studied in terms of the Stokes Time and the density fraction $\beta$. The relation number between both kind of particles and also the role that this parameter has on the synchronization was study in terms of the Kuramoto order parameter.

The full content of the article can be consulted on `https://journals.aps.org/pre/abstract/10.1103/PhysRevE.94.013103`

## 4.5 Conclusion

Lagrangian analysis provides an excellent tool to summarize the collective motion of particles. The FTLE has been shown as a useful tool to explore numerically the invariant manifolds and coherent structures for high order dimensional systems. Its spatial distribution has revealed the importance of dissipative and dumping effects over different kinds of particles, shaping the coherent structures and the invariant manifolds as main cores of trajectory organization and dynamics segregation. Ridges on this sensitivity field act as separatrices, similar to LCSs, partitioning the corresponding subspace.

The parameter analysis and perturbation of initial conditions to observe its influence on the particle motion have been analyzed through the FTLE distribution; ridges in the FTLE field at each spatial point partition phase space into zones of different dynamics. This is enhanced mainly in regions with a high variability on the velocity field where there are flow structures such as strain, eddies, or shear regions; we observe how particles located on either side of the shear area will evolve to different spatial locations after a short time. The same has been shown for the non-rigid particles: bubbles and reactive particles. Increasing the radius, and hence, reinforcing the inertial effects, will lead to changes in the FTLE pattern.

The coalescence effect is an irreversible process where two bubbles collapse into one, and it cannot be studied in FTLE terms due to the fact that at any collision point at a finite time for neighboring particles their FTLE remains zero. In this case, measuring the rate, the number of collisions, and how they depend on initial properties was studied through adimensional number $R_0/d_0$, showing that the collision rate follows a Levy distribution, where its shape highly depends on this dimensionless factor.

The synchronization between reactive particles; Lagrangian (chemicals) and inertial particles (beads), depends on system parameters and also on the ratio between both types of particles. Patches of oscillating and nonoscillating particles were found on the domain. The non-synchronized areas show an agreement with regions separated by the transport barriers revealed by ridges of the FTLE.

This study can be extended to any other kinds of particle which require more dimensions to describe their states. Also, the parameters introduced here to describe the particle motion can be extended to other non-analytical flows. This dependence can be exploited to make particles of different sizes cluster in different regions of the fluid and thus separate and segregate them.

# Chapter 5

# Advective transport on a Von Karman flow

## 5.1 Introduction

In this section, the trajectories solution of the equation Eq. (1.8), come from real experimental data obtained with image visualization techniques. This produces sequences of pictures of real particles transported under the action of a flow captured with high-speed cameras. Here, the data obtained correspond to the trajectories inside an isotropic turbulent flow using the novel Lagrangian Particle Tracking (LPT) algorithm Shake-The-Box (STB) [76]. This section is intended to summarize the basics of the experimental setup and show the first preliminary results. Due to the amount of data captured on the measuring campaign, most of the data are still under processing at Munich Supercomputer Center, and just a few test data are available, so here, we present a summary of the experiment carried out at the in the Göettingen Turbulence Facility 3 (GTF3) von Karman Flow Apparatus at the Max-Planck-Institute for Dynamics and Self-Organization (MPIDS) in collaboration between German Aerospace Center (DLR) and the University of Santiago de Compostela (USC). Part of the experiment described here has been used in the Jennifer Jucha thesis from earlier experiments [77].

## 5.2 Experimental setup

The flow visualization techniques are non-invasive experimental methods to measures physical properties of the fluid flow. These methods do not introduce any perturbation in the fluid flow due to the measuring processes. The fundamentals consist of injecting seeding particles into a fluid, illuminating the particles and recording them with capture devices. Then, the sequence of pictures are processed using mathematical methods to reconstruct the particle motion and extract the information related to its position, velocity and/or acceleration or other physical properties (rotation, radius...). Depending on the particle nature and its seeding density we can obtain information regarding the particles themselves or information regarding the flow. If there is a enough seeding particle density with a low Stokes number (1.11), they behave similarly to Lagrangian tracers and it is possible to obtain the flow velocity field. However, for particles where inertial effects are higher, the particle velocity is different from the fluid flow and we can not use them as tracers of the flow velocity field.

Here, we focus in a high turbulent flow generated by two counter-rotating propellers. To study the flow at lower Kolmogorov spatiotemporal scales, we require the use of high seeding

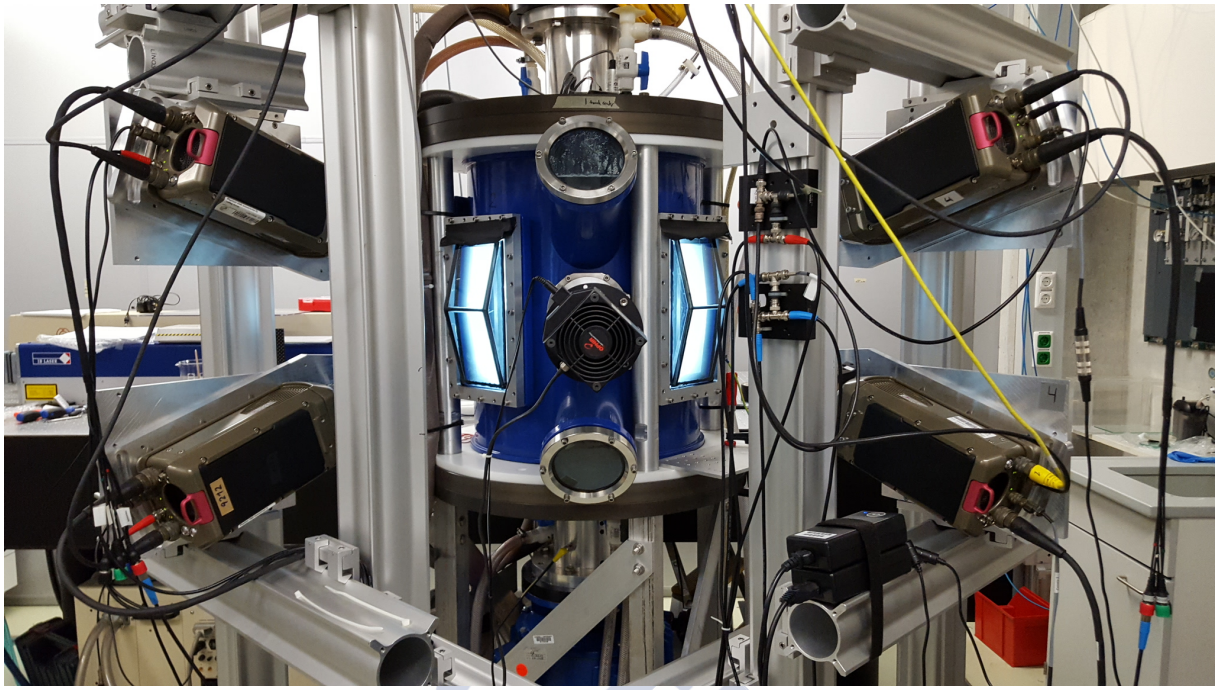

Figure 5.1: General view of the experimental setup. The 4 cameras look to the center of the water tank through the attached prisms.

density and four high-speed cameras together with power laser illumination to obtain the 3D trajectories. In the following section, we describe the experimental setup and the datasets obtained, followed by the results that are expected to be obtained.

**Capture device** The technical specifications of the capture device will depend on the flow characteristics. In turbulent flows, the Kolmogorov length and time microscales, $\eta$ and $\tau_\eta$ respectively, will be the lowest scales where viscosity dominates before turbulent kinetic energy is dissipated into heat. Depending on which scales of motion, and the corresponding flow features we want to capture, we have to ensure that, the capture device, has enough spatial and time resolution. On previous experiments [77], for the same flow configuration, the scales obtained were $\eta = 104\,\mu$m and $\tau_\eta = 10.0$ ms.

To capture the image sequence, 4 Phantom CMOS v640 high-speed cameras with an internal storage capacity of 32 Gb have been used. They have a maximum resolution of 2560x1600 pixels with a frame rate of 1400 fps with 12 bit depth. They are equipped with 100 mm Zeiss macro lenses ($f_\#$=16) and Scheimpflug adapters to record the particles in $\approx 45^\circ$ forward scattering. Prisms attached to the tank guarantee the camera windows are perpendicular to the camera axes. Three cameras are the minimum requirement to get the 3D position in space, the fourth camera is used to increase the precision of the measurement. The cameras can modify the resolution and the capture frame rate to adjust to the flow conditions.

With this frame rate capture ($\sim 0.701$ ms), we can ensure an oversample factor of $\sim 12.5$. However, this is not the case for the spatial scales, where the ratio pixel resolution is not the only factor. It depends also on the seeding density and hence the distance between particles, which should be enough to be distinguishable in the camera sensor.

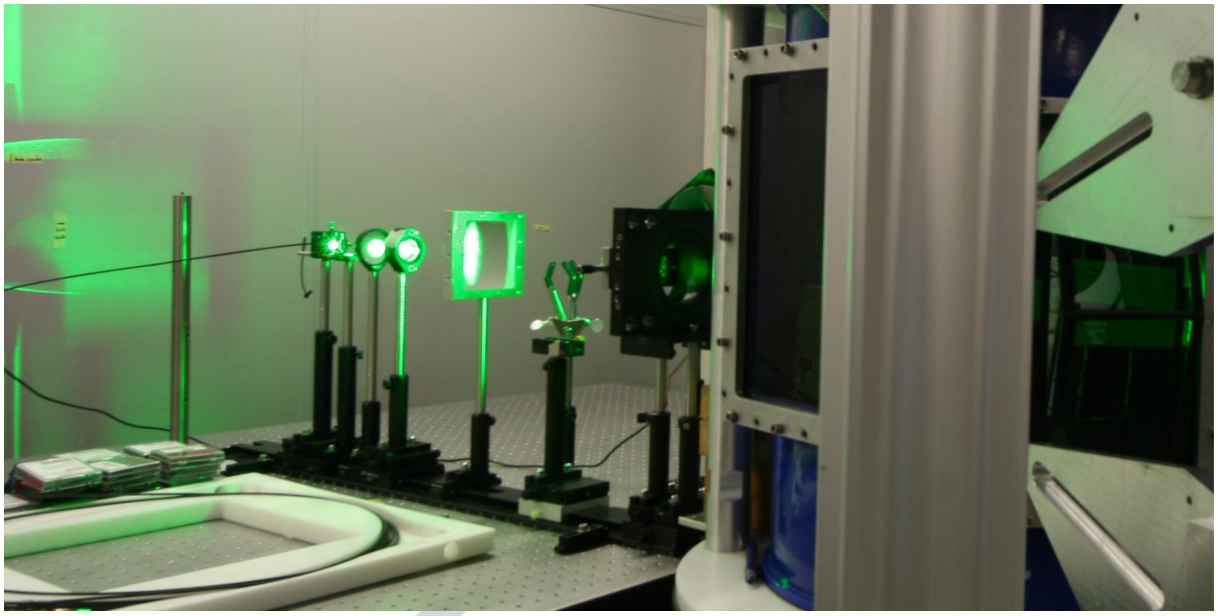

Figure 5.2: Optical setup to guide the laser inside the tank.

**Laser** The illumination should be close to uniform in intensity, due to the fact that all the particles must be illuminated with the same amount of light to have a Gaussian profile in terms of pixels, to be distinguishable in the image. Also, the illumination source must be synchronized with the camera capture framerate, in such a way that when the laser beam strikes the particles, the captured image does not include other sources of light, such as reflections or scattered light.

For the seeding illumination we use a fiber-coupled Nd:YAG laser (IB Chronos 400 MM IC SHG) with 10 kHz of frequency, a wavelength of 532 nm (green light) and an output power of 150 W. To synchronize the laser pulse with the cameras, the laser generates a clock pulse which is used as a synchronization signal for the 4 cameras to capture the same picture at the same time instant after a light pulse is emitted.

The laser beam is conducted to the water tank through an optical lens system as shown in Fig. (5.2). It is made by a divergent lens which opens the beam and a cylindrical one, which expands it in the vertical axis direction to generate an elliptic Gaussian beam with an uniform power density in the center of the ellipse area. Then, a rectangular area inside the Gaussian ellipse is removed with a knife edge to generate a rectangular beam to illuminate uniformly the center of the tank where the homogeneous turbulence takes place (Fig. (5.3)(c)) . The maximum volume illuminated was intended to be of $50\times50\times20\,\mathrm{mm}^2$.

**Seeding** Two types of seeding have been used, both of them are spherical particles. The seeding is inserted into the tank by a syringe with a diluted water-alcohol solution through a small valve aperture on the top. The first one is made of polystyrene, transparent with a diameter of 20 $\mu$m, with a density of $\rho$=1.05g/cm$^3$. These particles are intended to be Lagrangian due to their low radius and a density close to that of water to avoid flotation effects. The second type has a bigger diameter range, between 106-125 $\mu$m and a density of $\rho$=1.003 g/cm$^3$.

**Von Karman turbine** The flow chamber shown in Fig.(5.3)(a) is made of stainless steel. It has a height of 58 cm and an inner diameter of 40 cm filled with deionized water. Inside,

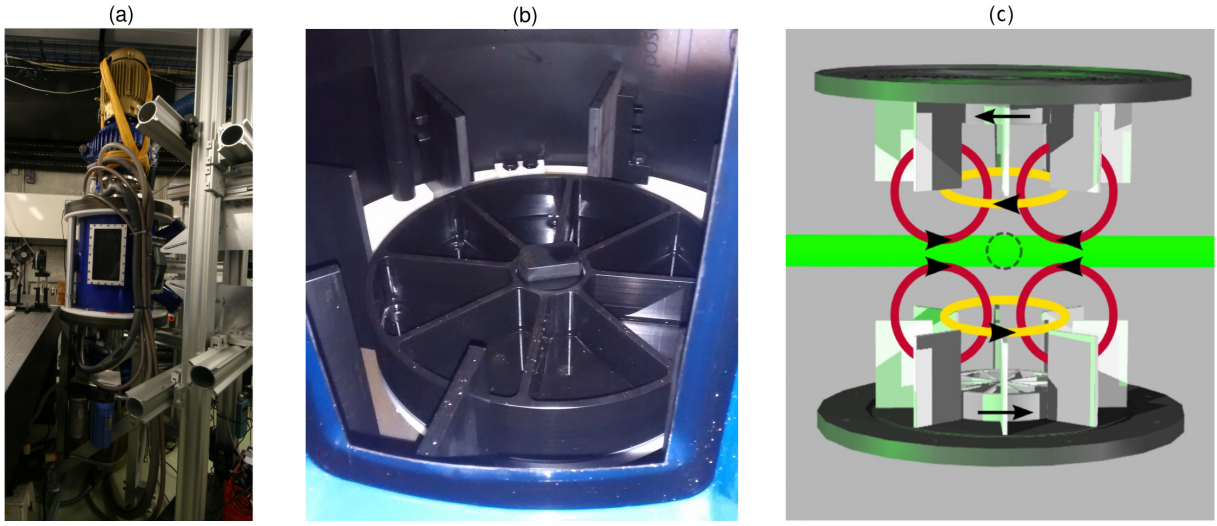


Figure 5.3: (a) Body of the von Karman turbine. Observe both engines at the top and the bottom. (b) Black propellers inside the water tank. (c) Scheme of the swirling flow generated inside the water tank (Modified from [77])

there are two counter-rotating (Fig. (5.3)(b-c)) propellers powered by two 7.5 kW engines. The frequency speed of the propellers is adjustable from 0.5 Hz to 1.5 Hz. The propellers have a wheel shape with a diameter of 25 cm and a height of 9 cm. Inside each wheel, there are 8 symmetrically distributed vanes. Between the wheels and the cylinder wall, there are eight plastic inserts to avoid any large-scale rotational flow, so at the center, there is a homogeneous turbulent region.

The inner wall was covered with a Plexiglass film to have cylindrical symmetric conditions and to avoid the generation of large-scale flow structure due to asymmetry created by unused window holes inside. The Plexiglas, the propellers, and the vans have been built in black material to diminish the internal light reflections and light scattering. The tank is cooled from the top and bottom by two plates, with a water pump circulation system. The temperature of the water was close to being constant at $21\pm5$ degrees to avoid convective effects. The air of the room is continuously re-filtered to remove dust particles and humidity from the air. To remove impurities from the deionized water, mainly due to material degradation, a pump with two filters for 30 $\mu$m and 5 $\mu$m is used. The filtering process avoids the introduction of impurities; particles different from the spherical seeding with a different light scattering pattern.

**Data collection** Each camera is individually connected with an Ethernet Gb to a switch connected to a Linux cluster via a glass fiber cable. To avoid bottlenecks the download process is done in parallel with each camera individually. For a propeller frequency of 0.5 Hz, two kinds of measures have been done. First, short sequences of pictures have been carried out to compute turbulence statistics. Then, long sequences of pictures (using the full camera capacity) are taken, to obtain the flow velocity to be able to compute integrated measures and explore the flow structures and their coherence.

Thus, 1000 time series of 200 time steps and 2000 time series of 40 time steps have been recorded to obtain converged statistics of velocity and acceleration, to compute the dissipation rate, the dissipation tensor, and statistics of the velocity gradient tensor, as well as (conditional) Eulerian and Lagrangian spatial and temporal correlation functions. For the analysis of pair and

tetraheds dispersion, 40 time series of 14000 time steps (full camera capacity) were recorded. A total amount of $\sim$40 Tb of particle image data have been collected. To compare the results for both particles another dataset of measures have been recorded with the bigger particles. After recording each sequence, we must wait a few seconds before taking another sequence to ensure the independence of the measure due to the randomness of turbulent flow.

Due to the repetitiveness of the process, it was automated with a master computer controlling the trigger signal to start the recording and stopping process and also the download process. After many recordings, the experiment is stopped to relax the laser and to check the seeding density. The whole data measurement campaign lasted two weeks (the download process takes 80 % of whole experiment data time campaign).

**LPT algorithm: Shake-The-Box** The Lagrangian Particle Tracking methods are intended to obtain the trajectories of individual particles. Originally these methods find the position of particles and then connect them to trajectories. The Shake-The-Box approach is able to identify and track individual particles at numbers of tens or even hundreds of thousands per time-step due to its exploitation of temporal information. This enables the processing of densely seeded flows (beyond 0.1 particles per pixel, ppp), which were previously reserved for tomographic PIV evaluations. A more detailed description of the method can be found in [78, 79, 76]

The core of the technique consists of: given a sequence of images, the positions of the particles are fit polynomially from $n-k$ to $n$ picture, then it is extrapolated to $n+1$. That is, it uses a prediction of the particle distribution for the subsequent time-step as a means to seize the temporal domain. Using the extrapolated position of the projected particle, this is shaken in order to find a matching particle. Errors introduced by the prediction process are corrected by an image matching technique ('shaking' the particle in space), followed by an iterative triangulation of particles newly entering the measurement domain. Then the shaken particles are removed to reduce the complexity in the following time steps. Trajectories of tracer particles are identified at high spatial accuracy due to a nearly complete suppression of ghost particles; a temporal filtering scheme further improves on accuracy and allows for the extraction of local velocity and acceleration as derivatives of a continuous function.

## 5.3 Expected results

Most of the hard processing, to turn the images obtained into particle trajectories with the Shake-The-Box algorithm and reconstruction of the Lagrangian path as it is shown in Fig.(5.4)(b), takes place at the München Supercomputer Center and at the DLR.

Once all the images are turned into manageable datasets of trajectories, the first step is to check the quality of the data, reproducing previous results obtained from [80], including Lagrangian and Eulerian velocity moments, and the Kolmogorov scales. Then, it is intended to compute converged statistics of velocity and acceleration, to compute the dissipation rate, the dissipation tensor, and statistics of the velocity gradient tensor, as well as (conditional) Eulerian and Lagrangian spatial and temporal correlation functions over particle dispersion or tetrads, among others. Also, the turbulence flow field will be studied in terms of FTLE analysis and Lagrangian Coherent Structures.

Using the turbulent flow field obtained with the Lagrangian particles $R = 20\mu$m, we will run simulations of ensembles of inertial particles. Then we will compare statistics relative to

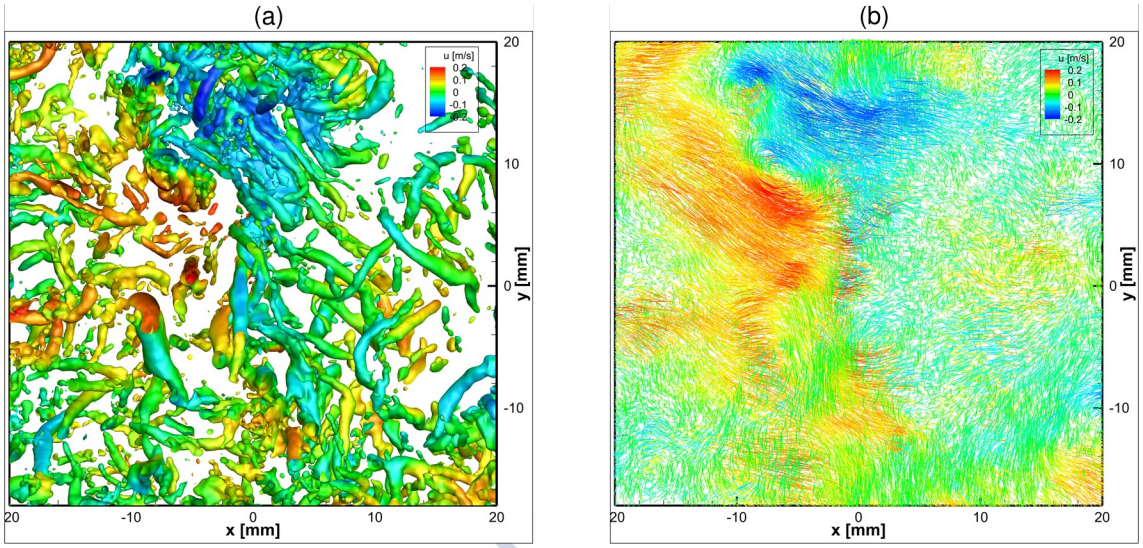


Figure 5.4: Preliminary results process from a sequence of pictures. (a) Isosurface of Q-Criteria=2500. (b) Particle trajectories colored by the x-velocity component. (Credits: Daniel Schanz, DLR)

velocity and acceleration with the results obtained from real inertial seeding $R = 120\,\mu$m. Also, we want to observe the role that smaller inertial forces play on the results, due to both particles having different Stokes numbers, and hence a different coupling with the fluid flow.

# Chapter 6

# Main Conclusions

Throughout this thesis we have used a dynamical systems approach to analyze different transport problems. The dynamical systems approach to transport in fluid flows focuses on the particle trajectories instead of mechanical aspects of fluid physics providing a powerful and versatile tool to analyze the transport and the fluid motion, especially through the concepts of invariant manifolds and Lyapunov exponents. These concepts have been applied to two transport problems with different natures: First, we have used a pure Lagrangian approach to study troposphere transport, to obtain information about the motion related to air masses themselves, focusing on a particular flow structure: Atmospheric Rivers. Then focusing on the evolution of mixing at climate scale and finally, the potential use of FTLE as a seasonal forecast variable for precipitation. Second, we have focused on the influence that inertial effects, have on particle motion for different kinds of spherical particles; rigid, bubbles and reactive particles.

Measures of hyperbolicity such as the FTLE, extended to measure material stretching have been used to estimate the structures that organize transport: Lagrangian Coherent Structures. These can be estimated as maximal regions on the FTLE field differentiating the regions with different dynamics. Finally the main conclusions of this work can be summarized as:

- We identified the Atmospheric river as an attracting Lagrangian Coherent Structure. We demonstrate that an Atmospheric River dominated by passive transport turns into the dominant hyperbolic attracting structure on the wind field, with a coherence of days.
- The summer anomalies of the FTLE analysis over the Atlantic region show a significant correlation with next winter's anomalies of precipitation. The same connection has been found for other circulation and temperature patterns.
- The climate analysis of the FTLE for the period 1979-2015 shows a link between climate variability and mixing process with a scale of days. Also, the impact of ARs on mixing plays a key role in regional climate.
- We demonstrate that the use of higher-order dimensional methods to compute the FTLE can capture the sensitiveness of initial velocity plays on inertial particles for those areas where there is a intense flow variability.
- Time dependent particle size plays a key role in the formation of coherent structures and flow partitioning. The effect of merging has its highest influence on neighboring bubbles and their size. It increases the collision rate in the first moments, and reduces as the flow evolves, following a Levy distribution.

- The particle parameters modified the exchange of chemical properties. The presence of transport barriers affect to synchronization of chemical oscillators, leading to patches of oscillating and nonoscillating particles
- The LPT Shake-The-Box algorithm, increases by many orders the number of particles resolved, even for high Reynolds turbulent fluid flows in comparison with previous techniques such as Tomographic PIV. We tracked up to 70,000 particles in a volume of $50\times50\times15$ mm$^3$ with a mean inter-particle distance lower than 7 Kolmogorov lengths in a Von Karman flow with a $Re_\lambda = 350\mu$m.

# Chapter 7

# Bibliography


[1] D. Tsumune, T. Tsubono, M. Aoyama, and K. Hirose, "Distribution of oceanic137Cs from the Fukushima Dai-ichi Nuclear Power Plant simulated numerically by a regional ocean model," *Journal of Environmental Radioactivity*, vol. 111, pp. 100–108, sep 2012.

[2] K. O. Buesseler, S. R. Jayne, N. S. Fisher, I. I. Rypina, H. Baumann, Z. Baumann, C. F. Breier, E. M. Douglass, J. George, A. M. Macdonald, H. Miyamoto, J. Nishikawa, S. M. Pike, and S. Yoshida, "Fukushima-derived radionuclides in the ocean and biota off Japan," *Proceedings of the National Academy of Sciences*, vol. 109, no. 16, pp. 5984–5988, apr 2012.

[3] K. Buesseler, M. Aoyama, and M. Fukasawa, "Impacts of the Fukushima nuclear power plants on marine radioactivity," *Environmental Science and Technology*, vol. 45, no. 23, pp. 9931–9935, dec 2011.

[4] M. McNutt, "The hunt for MH370," *Science*, vol. 344, no. 6187, p. 947, may 2014.

[5] E. Jansen, G. Coppini, and N. Pinardi, "Drift simulation of MH370 debris using superensemble techniques," *Natural Hazards and Earth System Sciences*, vol. 16, no. 7, pp. 1623–1628, 2016.

[6] E. N. Lorenz, "Deterministic Nonperiodic Flow," *Journal of the Atmospheric Sciences*, vol. 20, no. 2, pp. 130–141, mar 1963.

[7] T. Peacock and G. Haller, "Lagrangian coherent structures: The hidden skeleton of fluid flows," *Physics Today*, vol. 66, no. 2, pp. 41–47, 2013.

[8] S. H. Strogatz, "Nonlinear dynamics and chaos: with applications to physics, biology and chemistry," *Book*, p. 498, 1994.

[9] S. C. Shadden, "Lagrangian Coherent Structures," in *Transport and Mixing in Laminar Flows: From Microfluidics to Oceanic Currents*. Weinheim, Germany: Wiley-VCH Verlag GmbH & Co. KGaA, nov 2011, pp. 59–89.

[10] V. Rom-Kedar, A. Leonard, and S. Wiggins, "An analytical study of transport, mixing and chaos in an unsteady vortical flow," *Journal of Fluid Mechanics*, vol. 214, no. -1, pp. 347–394, may 1990.

[11] G. Haller and G. Yuan, "Lagrangian coherent structures and mixing in two-dimensional turbulence," *Physica D: Nonlinear Phenomena*, vol. 147, no. 3-4, pp. 352–370, dec 2000.

[12] R. T. Pierrehumbert, "Large-scale horizontal mixing in planetary atmospheres," *Physics of Fluids A*, vol. 3, no. 5, pp. 1250–1260, may 1991.

[13] R. T. Pierrehumbert and H. Yang, "Global Chaotic Mixing on Isentropic Surfaces," *Journal of the Atmospheric Sciences*, vol. 50, no. 15, pp. 2462–2480, aug 1993.

[14] J. Von Hardenberg, K. Fraedrich, F. Lunkeit, and A. Provenzale, "Transient chaotic mixing during a baroclinic life cycle," *Chaos*, vol. 10, no. 1, pp. 122–134, mar 2000.

[15] F. J. Beron-Vera, M. J. Olascoaga, M. G. Brown, H. Koçak, and I. I. Rypina, "Invariant-tori-like Lagrangian coherent structures in geophysical flows," *Chaos*, vol. 20, no. 1, p. 017514, mar 2010.

[16] W. Tang, M. Mathur, G. Haller, D. C. Hahn, and F. H. Ruggiero, "Lagrangian Coherent Structures near a Subtropical Jet Stream," *Journal of the Atmospheric Sciences*, vol. 67, no. 7, pp. 2307–2319, jul 2010.

[17] B. Rutherford, G. Dangelmayr, J. Persing, M. Kirby, and M. T. Montgomery, "Lagrangian mixing in an axisymmetric hurricane model," *Atmospheric Chemistry and Physics*, vol. 10, no. 14, pp. 6777–6791, jul 2010.

[18] T. Y. Koh and B. Legras, "Hyperbolic lines and the stratospheric polar vortex," *Chaos*, vol. 12, no. 2, pp. 382–394, jun 2002.

[19] I. I. Rypina, M. G. Brown, F. J. Beron-Vera, H. Koçak, M. J. Olascoaga, and I. A. Udovydchenkov, "On the Lagrangian Dynamics of Atmospheric Zonal Jets and the Permeability of the Stratospheric Polar Vortex," *Journal of the Atmospheric Sciences*, vol. 64, no. 10, pp. 3595–3610, oct 2007.

[20] A. de la Cámara, C. R. Mechoso, K. Ide, R. Walterscheid, and G. Schubert, "Polar night vortex breakdown and large-scale stirring in the southern stratosphere," *Climate Dynamics*, vol. 35, no. 6, pp. 965–975, nov 2010.

[21] T. Sapsis and G. Haller, "Inertial Particle Dynamics in a Hurricane," *Journal of the Atmospheric Sciences*, vol. 66, no. 8, pp. 2481–2492, aug 2009.

[22] P. C. du Toit and J. E. Marsden, "Horseshoes in hurricanes," *Journal of Fixed Point Theory and Applications*, vol. 7, no. 2, pp. 351–384, oct 2010.

[23] B. Rutherford, G. Dangelmayr, J. Persing, W. H. Schubert, and M. T. Montgomery, "Advective mixing in a nondivergent barotropic hurricane model," *Atmospheric Chemistry and Physics*, vol. 10, no. 2, pp. 475–497, jan 2010.

[24] B. Rutherford, G. Dangelmayr, and M. T. Montgomery, "Lagrangian coherent structures in tropical cyclone intensification," *Atmospheric Chemistry and Physics*, vol. 12, no. 12, pp. 5483–5507, 2012.

[25] W. Tang, G. Haller, J. J. Baik, and Y. H. Ryu, "Locating an atmospheric contamination source using slow manifolds," *Physics of Fluids*, vol. 21, no. 4, p. 043302, apr 2009.

[26] F. M. Ralph and M. D. Dettinger, "Storms, floods, and the science of atmospheric rivers," *Eos*, vol. 92, no. 32, pp. 265–266, 2011.

[27] P. J. Neiman, F. M. Ralph, G. A. Wick, J. D. Lundquist, and M. D. Dettinger, "Meteorological Characteristics and Overland Precipitation Impacts of Atmospheric Rivers Affecting the West Coast of North America Based on Eight Years of SSM/I Satellite Observations," *Journal of Hydrometeorology*, vol. 9, no. 1, pp. 22–47, 2008.

[28] L. Ruby Leung and Y. Qian, "Atmospheric rivers induced heavy precipitation and flooding in the western U.S. simulated by the WRF regional climate model," *Geophysical Research Letters*, vol. 36, no. 3, 2009.

[29] Y. Zhu and R. E. Newell, "Atmospheric rivers and bombs," *Geophysical Research Letters*, vol. 21, no. 18, pp. 1999–2002, 1994.

[30] D. A. Lavers and G. Villarini, "The nexus between atmospheric rivers and extreme precipitation across Europe," *Geophysical Research Letters*, vol. 40, no. 12, pp. 3259–3264, 2013.

[31] F. Santamaria, G. Boffetta, M. Martins Afonso, A. Mazzino, M. Onorato, and D. Pugliese, "Stokes drift for inertial particles transported by water waves," *Epl*, vol. 102, no. 1, p. 14003, apr 2013.

[32] G. Boffetta, F. De Lillo, and A. Gamba, "Large scale inhomogeneity of inertial particles in turbulent flows," *Physics of Fluids*, vol. 16, no. 4, 2004.

[33] G. Falkovich, A. Fouxon, and M. G. Stepanov, "Acceleration of rain initiation by cloud turbulence," *Nature*, vol. 419, no. 6903, pp. 151–154, 2002.

[34] M. C. Facchini, M. Mircea, S. Fuzzi, and R. J. Charlson, "Cloud albedo enhancement by surface-active organic solutes in growing droplets," *Nature*, vol. 401, no. 6750, pp. 257–259, sep 1999.

[35] J. Segurado, C. González, and J. LLorca, "A numerical investigation of the effect of particle clustering on the mechanical properties of composites," *Acta Materialia*, vol. 51, no. 8, pp. 2355–2369, 2003.

[36] T. Haszpra and T. Tél, "Volcanic ash in the free atmosphere: A dynamical systems approach," in *Journal of Physics: Conference Series*, vol. 333, no. 1, 2011.

[37] S. A. ISARD, S. H. GAGE, P. COMTOIS, and J. M. RUSSO, "Principles of the Atmospheric Pathway for Invasive Species Applied to Soybean Rust," *BioScience*, vol. 55, no. 10, p. 851, 2005.

[38] D. G. Schmale, D. A. Shah, and G. C. Bergstrom, "Spatial Patterns of Viable Spore Deposition of Gibberella zeae in Wheat Fields," *Phytopathology*, vol. 95, no. 5, pp. 472–479, 2005.

[39] A. Bracco, P. H. Chavanis, A. Provenzale, and E. A. Spiegel, "Particle aggregation in a turbulent Keplerian flow," *Physics of Fluids*, vol. 11, no. 8, pp. 2280–2287, 1999.

[40] H. Ruan, M. Jang, and C. Yang, "Optical focusing inside scattering media with time-reversed ultrasound microbubble encoded light," *Nature Communications*, vol. 6, 2015.

[41] R. Terzano, M. Spagnuolo, L. Medici, F. Tateo, and P. Ruggiero, "Characterization of Different Coal Fly Ashes for Their Application in the Synthesis of Zeolite X As Cation Exchanger for Soil Remediation Characterization of Different Coal Fly Ashes for Their Application in the Synthesis of Zeolite X As Cation Exchanger ," *Fresenius Environmental Bulletin*, vol. 14, no. 4, pp. 263–267, 2005.

[42] S. L. Wright, D. Rowe, R. C. Thompson, and T. S. Galloway, "Microplastic ingestion decreases energy reserves in marine worms," *Current Biology*, vol. 23, no. 23, 2013.

[43] OpenPIV, "Open source Particle Image Velocimetry," Retrieved from http://openptv-python.readthedocs.io/en/latest/intro.html.

[44] M. R. Maxey and J. J. Riley, "Equation of motion for a small rigid sphere in a nonuniform flow," *Physics of Fluids*, vol. 26, no. 4, pp. 883–889, 1983.

[45] R. Gatignol, "The FAXEN FORMULAE FOR A RIGID PARTICLE IN AN UNSTEADY NON-UNIFORM STOKES FLOW," *Journal de Mecanique Theorique et Appliquee*, vol. 2, no. 2, pp. 143–160, 1983.

[46] E. E. Michaelides, "Hydrodynamic Force and Heat/Mass Transfer From Particles, Bubbles, and Drops—The Freeman Scholar Lecture," *Journal of Fluids Engineering*, vol. 125, no. 2, p. 209, 2003.

[47] J. Magnaudet and D. Legendre, "The viscous drag force on a spherical bubble with a time-dependent radius," *Physics of Fluids*, vol. 10, no. 3, pp. 550–554, 1998.

[48] Z. Zapryanov and S. Tabakova, *Dynamics of Bubble, Drops and Rigid Particles*. Springer Science & Business Media, 1999, vol. 50.

[49] S. Sangal, M. K. Singhal, and R. P. Saini, "Hydro-abrasive erosion in hydro turbines: a review," *International Journal of Green Energy*, vol. 15, no. 4, pp. 232–253, 2018.

[50] D. P. Dee, S. M. Uppala, A. J. Simmons, P. Berrisford, P. Poli, S. Kobayashi, U. Andrae, M. A. Balmaseda, G. Balsamo, P. Bauer, P. Bechtold, A. C. Beljaars, L. van de Berg, J. Bidlot, N. Bormann, C. Delsol, R. Dragani, M. Fuentes, A. J. Geer, L. Haimberger, S. B. Healy, H. Hersbach, E. V. Hólm, L. Isaksen, P. Kållberg, M. Köhler, M. Matricardi, A. P. Mcnally, B. M. Monge-Sanz, J. J. Morcrette, B. K. Park, C. Peubey, P. de Rosnay, C. Tavolato, J. N. Thépaut, and F. Vitart, "The ERA-Interim reanalysis: Configuration and performance of the data assimilation system," *Quarterly Journal of the Royal Meteorological Society*, vol. 137, no. 656, pp. 553–597, 2011.

[51] P. D. Miller, C. K. Jones, A. M. Rogerson, and L. J. Pratt, "Quantifying transport in numerically generated velocity fields," *Physica D: Nonlinear Phenomena*, vol. 110, no. 1-2, pp. 105–122, dec 1997.

[52] G. Haller and A. C. Poje, "Finite time transport in aperiodic flows," *Physica D: Nonlinear Phenomena*, vol. 119, no. 3-4, pp. 352–380, aug 1998.

[53] K. Ide, D. Small, and S. Wiggins, "Distinguished hyperbolic trajectories in time-dependent fluid flows: analytical and computational approach for velocity fields defined as data sets," *Nonlinear Processes in Geophysics*, vol. 9, no. 3/4, pp. 237–263, 2002.

[54] S. Wiggins, *Normally hyperbolic invariant manifolds in dynamical systems*, ser. Applied Mathematical Sciences. New York, NY: Springer New York, 1994, vol. 105.

[55] G. Froyland, K. Padberg, M. H. England, and A. M. Treguier, "Detection of coherent oceanic structures via transfer operators," *Physical Review Letters*, vol. 98, no. 22, p. 224503, may 2007.

[56] G. Froyland and K. Padberg, "Almost-invariant sets and invariant manifolds - Connecting probabilistic and geometric descriptions of coherent structures in flows," *Physica D: Nonlinear Phenomena*, vol. 238, no. 16, pp. 1507–1523, aug 2009.

[57] G. Haller, "A variational theory of hyperbolic Lagrangian Coherent Structures," *Physica D: Nonlinear Phenomena*, vol. 240, no. 7, pp. 574–598, mar 2011.

[58] A. Okubo, "Horizontal dispersion of floatable particles in the vicinity of velocity singularities such as convergences," *Deep-Sea Research and Oceanographic Abstracts*, vol. 17, no. 3, pp. 445–454, 1970.

[59] J. Weiss, "The dynamics of enstrophy transfer in two-dimensional hydrodynamics," *Physica D: Nonlinear Phenomena*, vol. 48, no. 2-3, pp. 273–294, 1991.

[60] J. C. R. Hunt, a. a. Wray, and P. Moin, "Eddies, streams, and convergence zones in turbulent flows," in *Center for Turbulence Research, Proceedings of the Summer Program*, no. 1970, 1988, pp. 193–208.

[61] G. Haller, "Lagrangian coherent structures from approximate velocity data," *Physics of Fluids*, vol. 14, no. 6, pp. 1851–1861, jun 2002.

[62] S. C. Shadden, F. Lekien, and J. E. Marsden, "Definition and properties of Lagrangian coherent structures: Mixing and transport in two-dimensional aperiodic flows," *Physica D*, vol. 212, pp. 271–304, 2005.

[63] F. Lekien, S. C. Shadden, and J. E. Marsden, "Lagrangian coherent structures in n-dimensional systems," *Journal of Mathematical Physics*, vol. 48, no. 6, p. 065404, jun 2007.

[64] S. C. Shadden, "Lagrangian Coherent Structures. Analysis of time-dependent dynamical systems using finite-time Lyapunov exponents." Retrieved from http://shaddenlab.berkeley.edu/uploads/LCS-tutorial/overview.html, 2005.

[65] G. Haller and F. J. Beron-Vera, "Geodesic theory of transport barriers in two-dimensional flows," *Physica D: Nonlinear Phenomena*, vol. 241, no. 20, pp. 1680–1702, oct 2012.

[66] F. Lekien, "Dynamically Consistent Lagrangian Coherent Structures," in *AIP Conference Proceedings*, vol. 742, no. 1. AIP, 2004, pp. 132–139.

[67] M. Branicki and S. Wiggins, "Finite-time Lagrangian transport analysis: Stable and unstable manifolds of hyperbolic trajectories and finite-time Lyapunov exponents," *Nonlinear Processes in Geophysics*, vol. 17, no. 1, pp. 1–36, jan 2010.

[68] M. Mathur, G. Haller, T. Peacock, J. E. Ruppert-Felsot, and H. L. Swinney, "Uncovering the Lagrangian skeleton of turbulence," *Physical Review Letters*, vol. 98, no. 14, p. 144502, apr 2007.

[69] G. Haller, "Lagrangian Coherent Structures," *Annual Review of Fluid Mechanics*, vol. 47, no. 1, pp. 137–162, 2015.

[70] M. Farazmand and G. Haller, "Polar rotation angle identifies elliptic islands in unsteady dynamical systems," *Physica D: Nonlinear Phenomena*, vol. 315, pp. 1–12, 2016.

[71] G. Haller, A. Hadjighasem, M. Farazmand, and F. Huhn, "Defining coherent vortices objectively from the vorticity," *Journal of Fluid Mechanics*, vol. 795, pp. 136–173, 2016.

[72] A. Hadjighasem, M. Farazmand, D. Blazevski, G. Froyland, and G. Haller, "A critical comparison of Lagrangian methods for coherent structure detection," *Chaos*, vol. 27, no. 5, 2017.

[73] A. Babiano, J. H. Cartwright, O. Piro, and A. Provenzale, "Dynamics of a small neutrally buoyant sphere in a fluid and targeting in Hamiltonian systems," *Physical Review Letters*, vol. 84, no. 25, pp. 5764–5767, 2000.

[74] I. J. Benczik, Z. Toroczkai, and T. Tél, "Selective Sensitivity of Open Chaotic Flows on Inertial Tracer Advection: Catching Particles with a Stick," *Physical Review Letters*, vol. 89, no. 16, p. 164501, sep 2002.

[75] P. Tallapragada and S. D. Ross, "Particle segregation by Stokes number for small neutrally buoyant spheres in a fluid," *Physical Review E - Statistical, Nonlinear, and Soft Matter Physics*, vol. 78, no. 3, 2008.

[76] D. Schanz, S. Gesemann, and A. Schröder, "Shake-The-Box: Lagrangian particle tracking at high particle image densities," *Experiments in Fluids*, vol. 57, no. 5, pp. 1–28, 2016.

[77] J. Jucha, "Time-Symmetry Breaking in Turbulent Multi-Particle Dispersion," Ph.D. dissertation, 2015.

[78] D. Schanz, A. Schröder, S. Gesemann, D. Michaelis, and B. Wieneke, "' Shake The Box ': A highly efficient and accurate Tomographic Particle Tracking Velocimetry ( TOMO-PTV ) method using prediction of particle positions," *10th International Symposium on Particle Image Velocimetry - PIV13. Delft, The Netherlands, July 1-3.*, pp. 1–13, 2013.

[79] D. Schanz, A. Schröder, and S. Gesemann, "'Shake The Box' - a 4D PTV algorithm: Accurate and ghostless reconstruction of Lagrangian tracks in densely seeded flows," *17th International Symposium on Applications of Laser Techniques to Fluid Mechanics*, pp. 7–10, 2014.

[80] J. Jucha, H. Xu, A. Pumir, and E. Bodenschatz, "Time-reversal-symmetry breaking in turbulence," *Physical Review Letters*, vol. 113, no. 5, pp. 1–5, 2014.

USC
UNIVERSIDADE
DE SANTIAGO
DE COMPOSTELA

# List of publications

- V. Pérez-Muñuzuri, J. Eiras-Barca, and D. Garaboa-Paz, "Tagging moisture sources with Lagrangian and inertial tracers: application to intense atmospheric river events," *Earth Syst. Dyn.*, vol. 9, no. 2, pp. 785–795, 2018.
- V. Pérez-Muñuzuri, D. Garaboa-Paz, and A. P. Muñuzuri, "Nonperfect mixing affects synchronization on a large number of chemical oscillators immersed in a chemically active time-dependent chaotic flow," *Phys. Rev. E*, vol. 94, no. 1, p. 13103, 2016.
- D. Garaboa-Paz, N. Lorenzo, and V. Pérez-Muñuzuri, "Influence of finite-time Lyapunov exponents on winter precipitation over the Iberian Peninsula," *Nonlinear Process. Geophys.*, vol. 24, no. 2, pp. 227–235, 2017.
- D. Garaboa-Paz, J. Eiras-Barca, and V. Pérez-Muñuzuri, "Climatology of Lyapunov exponents: The link between atmospheric rivers and large-scale mixing variability," *Earth Syst. Dyn.*, vol. 8, no. 3, pp. 865–873, 2017.
- J. Eiras-Barca, F. Dominguez, H. Hu, D. Garaboa-Paz, and G. Miguez-Macho, "Evaluation of the moisture sources in two extreme landfalling atmospheric river events using an Eulerian WRF tracers tool," *Earth Syst. Dyn.*, vol. 8, no. 4, pp. 1247–1261, 2017.
- D. Garaboa-Paz and V. Pérez-Muñuzuri, "A method to calculate finite-time Lyapunov exponents for inertial particles in incompressible flows," *Nonlinear Process. Geophys.*, vol. 22, no. 5, pp. 571–577, 2015.
- D. Garaboa-Paz, J. Eiras-Barca, F. Huhn, and V. Pérez-Muñuzuri, "Lagrangian coherent structures along atmospheric rivers," *Chaos*, vol. 25, no. 6, p. 063105, 2015.